Scale-Based Detection of Corners of Planar Curves

Anothai Rattarangsi and Roland T. Chin

Abstract—**A technique for detecting and localizing corners of planar curves is proposed. The technique is based on Gaussian scale space, which consists of the maxima of absolute curvature of the boundary function presented at all scales. The scale space of isolated simple and double corners is first analyzed to investigate the behavior of scale space due to smoothing and interactions between two adjacent corners. The analysis shows that the resulting scale space contains line patterns that either persist, terminate, or merge with a neighboring line. Next, the scale space is transformed into a tree that provides simple but concise representation of corners at multiple scales. Finally, a multiple-scale corner detection scheme is developed using a coarse-to-fine tree parsing technique. The parsing scheme is based on a stability criterion that states that the presence of a corner must concur with a curvature maximum observable at a majority of scales. Experiments were performed to show that the scale space corner detector is reliable for objects with multiple-size features and noisy boundaries and compares favorably with other corner detectors tested.**

Index Terms—**Corner detection, curvature scale space, digital curves, dominant point detection, Gaussian smoothing, multiresolution processing, scale space filtering.**

I. Introduction

DOMINANT points, having high curvature on the boundary of a planar object, often prove to be useful descriptive primitives. Such corner points, as observed by Attneave [3] in 1954, contain important information about the shape of an object.

Many algorithms have been developed to detect dominant corner points on *digital* curves. They work well if the object has similar size features and some information about its size is known *a priori*. The prior knowledge is required in the form of one or more input parameters to the algorithm. Since the object in question is assumed to be unknown, determination of the input parameters usually relies on trail-and-error procedures. Furthermore, in the presence of boundary noise, the input parameters must be chosen precisely to differentiate noise points from corner features.

The input parameters determine the region of support from which the curvature of the boundary is measured. Even if the input parameters are known for the determination of the region of support, the computation of local curvature measures based on this single region of support has been shown to be ineffective for objects with multiple-size features. These objects require varying regions of support for varying feature size. For example, a large region of support is required to measure the general shape of an object, such as a door key, and a small region might be needed to measure fine features, such as the teeth of the key.

Single-scale representation of objects usually leads either to missing fine features or to overlooking coarse features. Consequently, single-scale dominant point detection algorithms are unreliable because objects, in general, cannot categorically be assumed to have only features of a single size. Corner detection must therefore observe dominant points at both coarse and fine scales for the detection of corners at the most appropriate scales.

In this paper, we revisit the problem of dominant point detection on digital boundaries by integrating information obtained at multiple scales. The idea was based on the argument that curvature measurements of an object at different scales contain important information about physically significant features. The organization of the multiple-scale representation is adopted from the idea, introduced by Witkin in [21], of *scale space,* which has been applied to the smoothing of 1-D signals where the signal is presented across a continuum of scales and where zero crossings of a function of the signal are mapped onto a scale-versus-location space. The map in [21] is then used to determine individual regions and their corresponding scales for the purpose of signal smoothing; hence, different amounts of smoothing are applied to different regions.

In this paper, we present a scale-based dominant point detection algorithm that uses a multiple-scale representation of the boundary and a multiple-scale searching procedure. In Section II, we survey various existing dominant point detection algorithms and their relation to scale space filtering. In Section III, we present the construction of a scale space map that consists of local maxima of absolute curvature of the boundary. Properties of this map are investigated in Section IV. The results enable us to understand the map precisely and to develop a computational procedure for the detection of dominant points. In Section V, the digital implementation of the scale space map is addressed, and a tree parsing for corners is presented. Experimental results, including noise sensitivity and an extensive comparative study, are presented in Section VI.

II. Background

Most existing dominant point detectors are single-scale algorithms that work well if the object has similar size features and some information about its size is known *a priori*. Examples of this type of corner detectors include

Manuscript received November 3, 1989; revised June 18, 1991. This work was supported by the National Science Foundation under Grant ECS-8352356 and by General Motors Research Foundations. Recommended for acceptance by R. Woodham.

A. Rattarangsi was with the Department of Electrical and Computer Engineering, University of Wisconsin, Madison, WI 53706. He is now with the Electrical and Electronic Department, Royal Thai Navy, Bangkok, Thailand.

R. T. Chin is with the Department of Electrical and Computer Engineering, University of Wisconsin, Madison, WI 53706.

IEEE Log Number 9104988.

those of Rosenfeld-Johnston [15], Rosenfeld-Weszka [16], Anderson-Bezdek [1], and Freeman-Davis [8]; all require prior knowledge in the form of input parameters.

Sankar and Sharma [18] introduced an algorithm that does not require any input parameter and has the flavor of multiple-scale processing. Instead of attempting to estimate curvature at every point on a boundary, the approach assigns one of the three integers $+1$, -1, or 0 to each point if its curvature is positive, negative, or 0, respectively. Then, the algorithm iteratively averages the assigned value at each point with its immediate neighbors. Points with maximum averaged values within their local neighbors are detected as corners at the end of the iteration.

In [20], Teh and Chin introduced a parameter-free corner detector that is similar to the Rosenfeld-Johnston, Rosenfeld-Weszka, and Freeman-Davis algorithms; however, the region of support for the computation of local curvature at each boundary point is adaptively determined based on local properties of the point. The idea was adopted from the remark by Langride [9] that each boundary point has its own view of the curve. The algorithm has shown to work well with objects with multiple-size features. However, it has been shown to generate redundant corners when the object is corrupted with quantization and boundary noise.

Saint-Marc and Medioni [17] suggested the iterative smoothing of a boundary curve for feature extraction. The smoothing is done using a decaying exponential window that is a function of a predetermined smoothing parameter and the local gradient of the point in question. The smoothing is designed to preserve discontinuities of the boundary. The discontinuities remaining after the smoothing process are considered to be corners. However, the results are sensitive to the smoothing parameter; too large a value will blur every corner, and too small a value will detect many false alarms. A procedure to determine the proper smoothing parameter has not been suggested, and the various smoothed boundary signals have not been utilized in the detection.

Recently, Meer *et al.* [12] suggested a method to detect dominant points by first determining the optimal scale of a Gaussian-like convolution multiple-scale representation of the boundary. Then, a measure of optimality, which is directly proportional to the total curvature of the boundary, is defined. The optimal scale is determined such that the difference in the measure of optimality between two successive scales is smallest. Subsequently, corners are detected at this optimal scale. The method uses a single scale that best represents the object. However, it implicitly suggests that there exists a single scale that is more important than others.

In [2], Asada and Brady proposed the curvature primal sketch to represent changes in boundary curvature. The primal sketch consists of various symbolic descriptions at multiple scales, such as corners, knots, and ends, and is generated by convolving different size Gaussian windows with the curvature and tracking the locations of curvature discontinuities. Boundary symbolic features are each detected at a different scale based on some preconceived notions of a best scale for a particular feature. The resulting representation is a multiple-scale interpretation of the boundary; however, the detection of an individual symbolic feature is still based on the signal at a single scale.

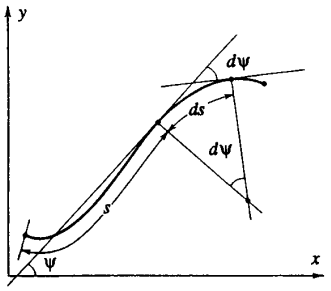

Fig. 1. Intrinsic definition of a curve.

It is reasonable to believe that the problem of corner detection could be solved effectively by utilizing curvature information at various scales in a multiple-scale boundary representation. The scale space of Witkin [21] provides such a representation. Moreover, theoretical studies have been conducted to investigate the behavior of the scale space; see [22], [19], [14], [4], and [7]. They have shown that the scale space pattern, under certain assumptions, possesses nice properties suitable for the filtering of signals. However, the scale space of Witkin cannot be directly applied to detect corners. This is because it represents points of inflection of 1-D signal for noise cleaning, whereas in the case of corner detection, the scale space must represent the maxima of absolute curvature of a 2-D boundary function. The scale space of a 2-D boundary function can be generated by convolving a varying-scale Gaussian smoothing function with the boundary functions in both the x and y directions separately. Such a multiple-scale representation of the boundary function of a planar object, called the curvature scale space, has been used in [13] for the detection of zero-curvature boundary points for object recognition. In the following, the construction of the scale space of maxima of absolute curvature is presented, and the detection of corners by searching for consistent maxima of absolute curvature in this space is proposed.

III. Scale Space Description of Corners

Corners of a planar curve correspond to points of high curvature. In order to construct a scale space map of corners, it is necessary to use a representation that allows the computation of the curvature and, subsequently, of its corners at varying levels of scale. Furthermore, the representation must be general enough to represent closed curves and multiple-value functions. Such a representation is to express the curve parametrically by its coordinate functions $x(s)$ and $y(s)$, where s is a path length variable along the curve; see Fig. 1. The curvature C at any point P on the curve is defined as the instantaneous rate of change of ψ, which is the angle subtended by the tangent at point P with the x axis, with respect to arc-length s, given by

$$C = \frac{\partial \psi}{\partial s}. \tag{3.1}$$

The curvature C can be defined in terms of the derivative of the functions $x(s)$ and $y(s)$ as

$$C(x,y) = \frac{\frac{\partial^2 y}{\partial x^2}}{\left[1 + \left(\frac{\partial y}{\partial x}\right)^2\right]^{3/2}}. \tag{3.2}$$

Let us denote

$$\dot{x} = \frac{\partial x}{\partial s} \qquad \dot{y} = \frac{\partial y}{\partial s} \qquad \ddot{x} = \frac{\partial^2 x}{\partial s^2} \qquad \ddot{y} = \frac{\partial^2 y}{\partial s^2}$$

then

$$\frac{\partial y}{\partial x} = \frac{\dot{y}}{\dot{x}} \qquad \frac{\partial^2 y}{\partial x^2} = \frac{\dot{x}\ddot{y} - \dot{y}\ddot{x}}{\dot{x}^3}.$$

Therefore, the curvature can be expressed in terms of $\dot{x}$, $\dot{y}$, $\ddot{x}$, and $\ddot{y}$ as

$$C(x,y) = \frac{\dot{x}\ddot{y} - \dot{y}\ddot{x}}{[\dot{x}^2 + \dot{y}^2]^{3/2}}. \tag{3.3}$$

Furthermore, the functions $x(s)$ and $y(s)$ must be related by

$$\frac{\partial x}{\partial s} = \cos\psi \qquad \frac{\partial y}{\partial s} = \sin\psi \tag{3.4}$$

which yields the curvature expression given by

$$C(x,y) = \dot{x}\ddot{y} - \dot{y}\ddot{x}. \tag{3.5}$$

To express the curvature at varying levels of detail, both boundary coordinate functions $x(s)$ and $y(s)$ are convolved with the Gaussian function $g(s,\sigma)$ defined by

$$g(s,\sigma) = \frac{1}{\sigma\sqrt{2\pi}} e^{-s^2/2\sigma^2} \tag{3.6}$$

where σ is the standard deviation of the distribution. The Gaussian function has been used by many others to generate multiple-scale signal representations. It decreases smoothly with distance and is differentiable and integrable. Let us assume for the time being that σ of the Gaussian function is small compared with the total length of the curve and that the curve in question is closed. The Gaussian-smoothed coordinate functions $X(s,\sigma)$ and $Y(s,\sigma)$ are defined by

$$X(s,\sigma) = \int_{u=s-S/2}^{u=s+S/2} x(u)\, g(s-u,\sigma)\, du \tag{3.7.1}$$

and

$$Y(s,\sigma) = \int_{u=s-S/2}^{u=s+S/2} y(u) g(s-u,\sigma)\, du \tag{3.7.2}$$

where S is the total length of the curve. The limit of the integration in (3.7) is to prevent the wrap-around effect of the convolving Gaussian function. In other words, the curvature function of the closed curve is assumed to be of finite duration, which avoids aliasing as a result of circular convolution in the Gaussian smoothing process if periodic function is used. This condition is also essential to the convergence of scale space [22], which guarantees that the number of zero crossings decreases as σ increases. It is to be noted that both $X(s,\sigma)$ and $Y(s,\sigma)$ are *smooth* functions since any derivative of $X(s,\sigma)$ is equal to the convolution of $x(s)$ with a Gaussian derivative of the same order. Hence, the curvature $C(s,\sigma)$ of a Gaussian-smoothed curve is readily given by applying $\dot{X}(s,\sigma), \dot{Y}(s,\sigma), \ddot{X}(s,\sigma)$, and $\ddot{Y}(s,\sigma)$ to (3.5).

To determine corners at a given scale σ, we solve for all the locations that have maximum absolute curvature, $|C(s,\sigma)|$, which are the positive maxima and negative minima of curvature. A scale space map of corners is then constructed by $\max_{s,\sigma} |C(s,\sigma)|$, which is equivalent to the following curvature optimization applied to each scale.

For $C(s,\sigma) > 0$, solve for the solutions $\{s_i\}$ in

$$\begin{aligned} \frac{\partial C(X(s,\sigma), Y(s,\sigma))}{\partial s} &= 0 \text{ subject to} \\ \frac{\partial^2 C(X(s,\sigma), Y(s,\sigma))}{\partial s^2} &< 0 \end{aligned} \tag{3.8.1}$$

and for $C(s,\sigma) < 0$, solve for the solutions $\{s_i\}$ in

$$\begin{aligned} \frac{\partial C(X(s,\sigma), Y(s,\sigma))}{\partial s} &= 0 \text{ subject to} \\ \frac{\partial^2 C(X(s,\sigma), Y(s,\sigma))}{\partial s^2} &> 0 \end{aligned} \tag{3.8.2}$$

where $\{s_i\}$ is the set of maxima of absolute curvature. In Fig. 2 a simple closed curve is shown at varying scales, their corresponding $X(s,\sigma)$ and $Y(s,\sigma)$, and the curvature computed by (3.5). In Fig. 3, the scale space map of the maxima of absolute curvature of the curve in Fig. 2, by solving (3.8) for $\{s_i\}$ at all σ starting from $\sigma = 0$, is shown. The line patterns of the map indicate the locations of the maxima through varying scales. Note that the sign of $C(s,\sigma)$ indicates the concavity[1] of the curve and provides useful information for the interpretation of the evolution of corners through scale. Therefore, on the s axis of the scale space map, a + sign indicates a concave upward corner (positive curvature) and a − sign indicates a concave downward corner (negative curvature).

It is evident from Fig. 3 that moving from fine to coarse scales, some existing maxima disappear, and some merge and become a single maximum. This suggests that rather than treating local curvature at one single scale, or at different scales as unrelated events, the scale space map can be used for corner detection as a multiple-scale problem.

In order to understand the behavior of the scale space map, we will investigate its properties using isolated simple and double corner models in the next section. These particular models allow us to study the scale space behavior of the relationship between two neighboring corners. Depending on the location and sharpness of the corners, and their interaction with adjacent corners, the line patterns of the scale space map may merge, disappear, repel, or attract each other as σ increases. This provides an organization of curvature information for the determination of corners, each at an appropriate scale.

[1] $C(s,\sigma)$ is positive at a point if, when traveling along the curve in the direction of increasing s, the curve is concave upward, and $C(s,\sigma)$ is negative if the curve is concave downward.

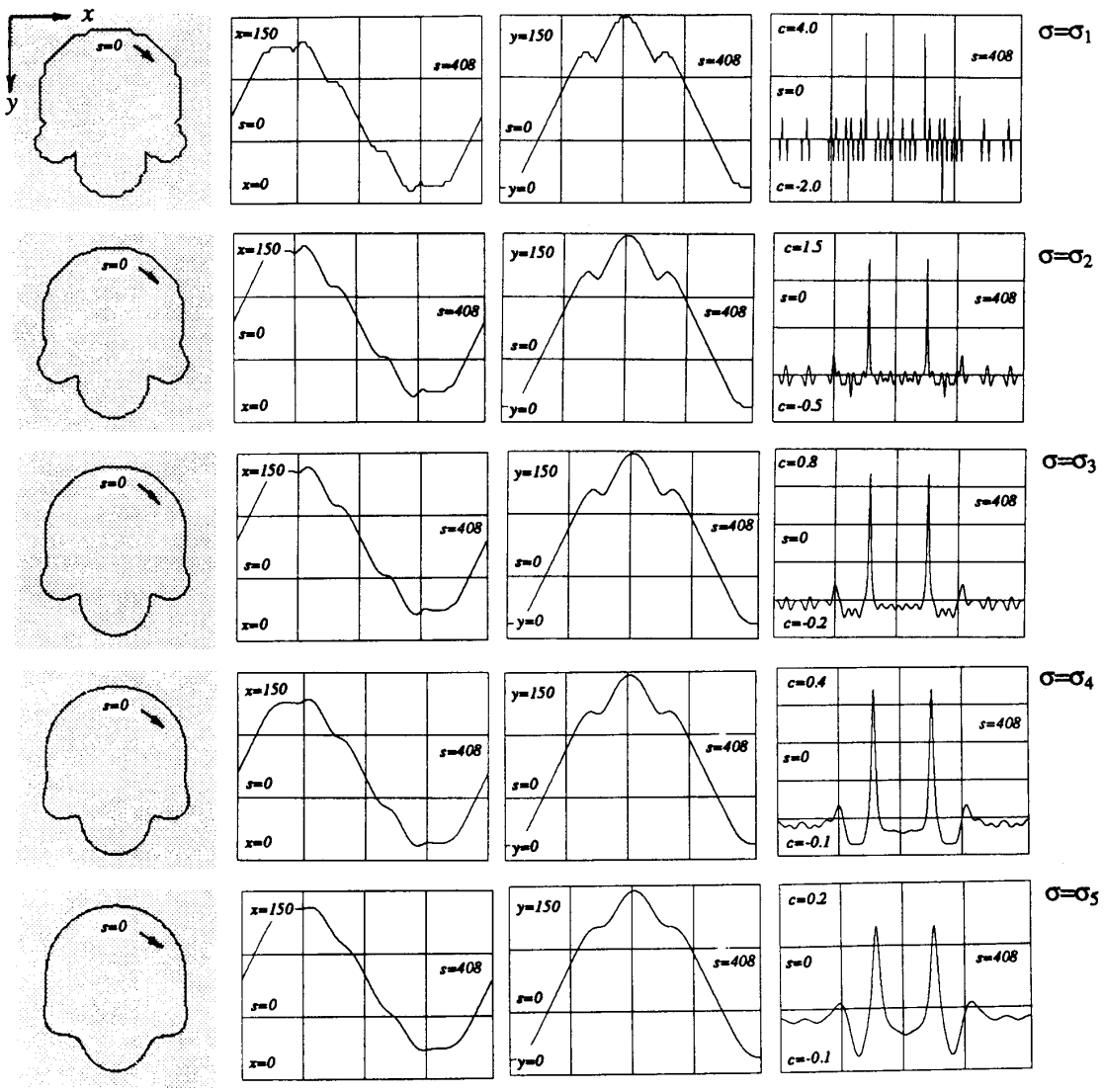

Fig. 2. First column: Simple closed curve from fine to coarse scales σ as a result of the Gaussian smoothing. Second column: $X(s,\sigma)$ with $s = 0$ as the point indicated in the image. Third column: $Y(s,\sigma)$. Fourth column: Curvature $C(s,\sigma)$. Note that $\sigma_1 < \sigma_2 < \sigma_3 < \sigma_4 < \sigma_5$.

IV. Analysis of Scale-Based Contour Models

The scale space map of maxima of absolute curvature[2] provides information on corner locations at varying scales. In this section, we will consider isolated single and double models [2] as shown in Fig. 4 to investigate the properties of the scale space map. These corner models are treated as isolated contours to simplify the investigation. The single corner Γ model is used to show the consistent behavior of the line patterns in the scale space map. The double corner END and STAIR models show the interaction between a pair of neighboring corners with respect to scale.

[2]The scale space of maxima of absolute curvature of a contour will be simply referred to as the *scale space map* throughout this paper. The maximum of absolute curvature of a boundary function will be referred to as *absolute maximum*.

In principle, a corner is affected by all its neighboring corners due to the Gaussian smoothing process. In order to simplify the scale space analysis, we assume that the scale space behavior of a corner is influenced only by its immediate neighbors and that other corners further away produce negligible effects on the corner in question. There is no explicit analysis of three or more corner models; however, properties derived from the double corner model analysis are used to deduce properties of higher order models. Subsequently, these properties are used to determine corners.

For a given scale σ, the curvature optimization in (3.8.1) or (3.8.2) can be rewritten as

$$\dot{X}(s,\sigma)\,\ddot{Y}(s,\sigma) - \dot{Y}(s,\sigma)\,\ddot{X}(s,\sigma) = 0 \qquad (4.1)$$

where a solution s is a curvature extremum. With the ap-

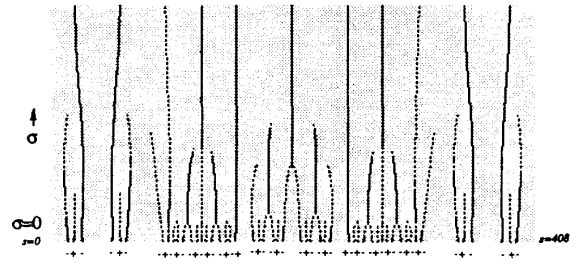

Fig. 3. Scale space map of maxima of absolute curvature. The horizontal axis is the arc length of the curve at $\sigma = 0$. The vertical axis is the Gaussian function parameter σ determining the degree of smoothing. The line pattern in the map represents the locations of the local maxima of the curvature. A + sign indicates downward concavity, and a − sign indicates upward concavity.

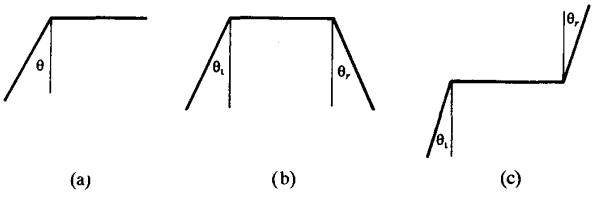

Fig. 4. Corner models: (a) Γ model; (b) END model; (c) STAIR model. The angles are allowed to vary independently.

propriate constraint, the set of curvature extrema is reduced to the set of maxima of absolute curvature that indicate corners. Let $F(s,\sigma)$ represent the function $X(s,\sigma)$ or $Y(s,\sigma)$. Since differentiation and convolution are commutative, the first derivative of the smoothed coordinate function $\dot{F}(s,\sigma)$ in (4.1) can be determined by

$$\dot{F}(s,\sigma) = \frac{\partial F(s,0) \ * \ g(s,\sigma)}{\partial s} = \frac{\partial F(s,0)}{\partial s} \ * \ g(s,\sigma) \quad (4.2)$$

where $*$ denotes convolution, and $F(s,0)$ is the unsmoothed coordinate function, that is, $\sigma = 0$. Likewise, $\ddot{F}(s,\sigma)$ in (4.1) can be determined by

$$\ddot{F}(s,\sigma) = \frac{\partial^3 F(s,0) \ * \ g(s,\sigma)}{\partial s^3} = \frac{\partial^2 F(s,0)}{\partial s^2} \ \frac{\partial g(s,0)}{\partial s} \quad (4.3)$$

where the derivative of $g(s,\sigma)$ with respect to s is given by

$$\dot{g}(s,\sigma) = \frac{\partial g(s,\sigma)}{\partial s} = \frac{-s}{\sigma^3\sqrt{2\pi}} e^{-s^2/2\sigma^2}. \quad (4.4)$$

Using (4.1) and the above derivatives, the scale space maps of the Γ, END, and STAIR models can be readily analyzed.

A. The Γ Model

Let us define, without loss of generality, a corner centered at the origin of the xy plane given by

$$X(s,0) = \begin{cases} s\sin\theta & \text{for } s < 0 \\ s & \text{for } s \geq 0 \end{cases} \quad (4.5)$$

$$Y(s,0) = \begin{cases} s\cos\theta & \text{for } s < 0 \\ 0 & \text{for } s \geq 0. \end{cases} \quad (4.6)$$

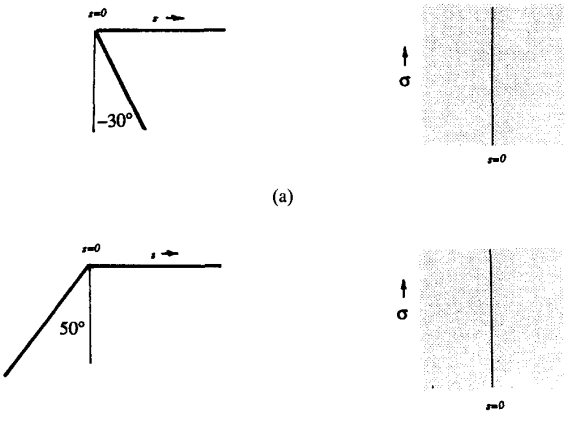

Fig. 5. Γ model produces a stationary and persistent scale space: (a) $\theta = -30°$ and its scale space map: (b) $\theta = -50°$ and its scale space map.

At $\sigma = 0$, both $\dot{X}(s,0)$ and $\dot{Y}(s,0)$ at the origin do not exist. At $\sigma \neq 0$, X and Y are n differentiable at all s. Using the derivative in (4.2) and (4.3) and the Γ model in (4.5) and (4.6), the curvature optimization of (4.1) becomes

$$-\cos\ \theta\ \dot{g}(s,\sigma) = 0. \quad (4.7)$$

At $\theta = 90°$, Γ becomes a straight line. In this case, any solution s will satisfy (4.7) but not the constraint of (3.8.2); hence, there is no absolute maximum. In the case of $\theta > -90°$ but not equal to 90°, (4.1) becomes

$$\dot{g}(s,\sigma) = 0.$$

Therefore, the only solution is at $s = 0$ independent of the corner angle θ, and the scale parameter σ. This produces a vertical line in scale space, that is, the absolute maxima occur at the same contour location independent of smoothing. This set of absolute maxima is said to be *stationary* in scale space. In addition, the line extends from $\sigma = 0$ to $\sigma = \infty$, that is, the maxima of absolute curvature exist at all scales and are said to be *persistent*. The model properties are summarized by Property 1. Two scale space maps determined analytically by solving the curvature optimization equation for absolute maxima are shown in Fig. 5.

Property 1: An isolated Γ model has a single stationary and persistent line pattern in scale space independent of θ and σ. □

B. The END Model

Let us consider another corner model, which consists of two corners θ_l and θ_r with the same concavity separated by a width of w; see Fig. 4(b). This END model at $\sigma = 0$ is given by

$$X(s,0) = \begin{cases} s\sin\theta_l & \text{for } s < 0 \\ s & \text{for } 0 \leq s < w \\ (s-w)\sin\theta_r + w & \text{for } s \geq w \end{cases} \quad (4.8)$$

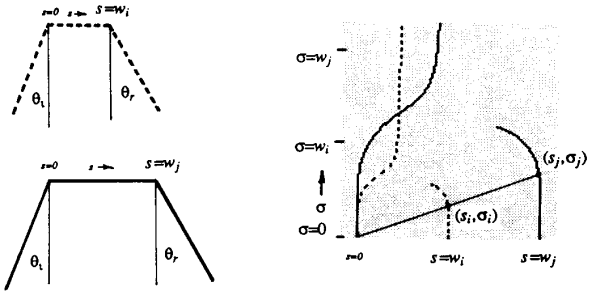

Fig. 6. Two END models with corner separations w_i and w_j and their corresponding scale space maps. The point (s_i, σ_i) belongs to the END model with $w = w_i$, and the point (s_j, σ_j) belongs to that with $w = w_j$. Both scale space patterns (solid and dash lines) are related by $s_j/s_i = \sigma_j/\sigma_i = w_j/w_i$.

$$Y(s,0) = \begin{cases} s\cos\theta_l & \text{for } s < 0 \\ 0 & \text{for } 0 \le s < w \\ -(s-w)\cos\theta_r & \text{for } s \ge w. \end{cases} \tag{4.9}$$

Using the derivatives in (4.2) and (4.3) and the END model equations, the curvature optimization (4.1) becomes (4.10) as shown at the bottom of the page. The set of absolute maxima $\{s_i\}$ of the above implicit equation at various values of σ forms the scale space map, which depends on the corner separation w and the corner angles θ_l and θ_r. Properties 2 to 6 summarize various properties of this model.

Property 2: The scale space map of an isolated END model with corner separation w_i is linearly related to the scale space map of another END model with corner separation w_j by the ratio of the separations given by w_i/w_j.

The above property depicts the effect of w on the scale space map. Let us fix θ_r and θ_l and vary w. First let s_i be a solution of (4.10) at $\sigma = \sigma_i$ of an END model with corner separation $w = w_i$. From (4.10), we obtained another solution $s_j = \frac{w_j}{w_i} s_i$ at $\sigma_j = \frac{w_j}{w_i}\sigma_i$ with corner separation $w = w_j$. Therefore, the ratio $s_i/s_j = w_i/w_j = \sigma_i/\sigma_j$ is a constant. In other words, the scale space maps of two END models, differing only by their corner separations, are linearly related by a scaling of w_i/w_j. Such a pair of END models is sketched in Fig. 6. □

To understand the effect of the corner angles θ_l and θ_r on the scale space map, two cases are considered: 1) $\theta_l + \theta_r > 0°$, that is, the two sides never intersect, and 2) $\theta_l + \theta_r < 0°$, that is, they intersect; see Fig. 7 for examples. It can be seen intuitively that case 1) will generate scale space line patterns consisting of two absolute maxima of the same concavity at each small value of σ. As σ increases, these absolute maxima will gradually move towards each other, and at a large enough σ, a single dominant absolute maximum of the original concavity will remain. In other words, the END model will smooth to consist of only one single corner. Depending on the relationship of two corners, the two absolute maxima will either merge to become one, or the sharper corner of the two will persist, whereas the weaker one will disappear. On the other hand, case 2) will generate two line patterns that repel each other. Variations of the END models are separately analyzed by the following properties.

The curvature optimization of the END model given by (4.10) under the condition of $\theta_l = \theta_r$ becomes

$$\frac{\dot{g}(s,\sigma)}{\dot{g}(s-\omega,\sigma)} = \frac{1 - 2\int_{-\infty}^{0} g(u-s,\sigma)\,du + 2\sin\theta\int_{-\infty}^{0} g(u-s,\sigma)\,du}{1 - 2\int_{-\infty}^{\omega} g(u-s,\sigma)\,du + 2\sin\theta\left\{1 - \int_{-\infty}^{\omega} g(u-s,\sigma)\,du\right\}}. \tag{4.11}$$

Property 3: An isolated right-angle END model has a stationary and persistent scale space map independent of σ.

For this case of $\theta_l = \theta_r = 0°$, which is a right-angle END model as shown in Fig. 8, the curvature optimization of (4.11) is simplified to

$$\frac{\dot{g}(s,\sigma)}{\dot{g}(s-\omega,\sigma)} = \frac{1 - 2\int_{-\infty}^{0} g(u-s,\sigma)\,du}{1 - 2\int_{-\infty}^{\omega} g(u-s,\sigma)\,du}. \tag{4.12}$$

To determine the maxima of absolute curvature at a particular σ, the solution in (4.12) must also satisfy the constraint of (3.8.1) and (3.8.2). The numerators of both sides of the equation are equal to 0 at $s = 0$ independent of σ; therefore, there is always a solution at $s = 0$ independent of σ. By the same token, another solution is at $s = w$. As in the case of the Γ model, the right-angle END model produces a pair of *stationary* absolute maxima at $s = 0$ and $s = w$. The scale

$$\frac{\dot{g}(s,\sigma)}{\dot{g}(s-\omega,\sigma)} = \frac{\cos\theta_r\left\{1 - 2\int_{-\infty}^{0} g(u-s,\sigma)\,du\right\} + \left\{\cos\theta_r + \sin\theta_l\cos\theta_r - \cos\theta_l + \sin\theta_r\cos\theta_l\right\}\int_{-\infty}^{0} g(u-s,\sigma)\,du}{\cos\theta_l\left\{1 - 2\int_{-\infty}^{w} g(u-s,\sigma)\,du\right\} + \left\{\cos\theta_l + \sin\theta_r\cos\theta_l - \cos\theta_r + \sin\theta_l\cos\theta_r\right\}\left\{1 - \int_{-\infty}^{\omega} g(u-s,\sigma)\,du\right\}}. \tag{4.10}$$

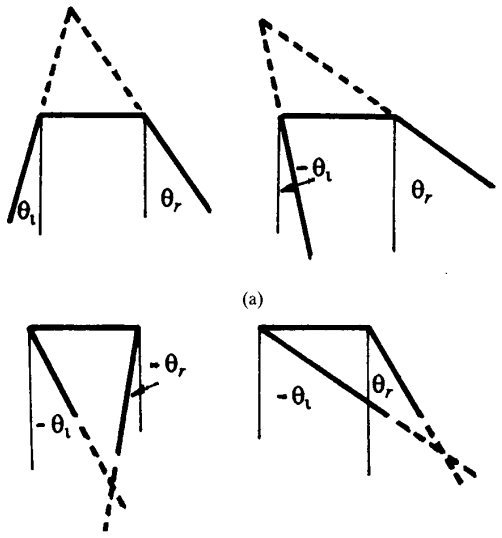

Fig. 7. (a) END model with $\theta_l + \theta_r > 0°$; (b) END model with $\theta_l + \theta_r < 0°$.

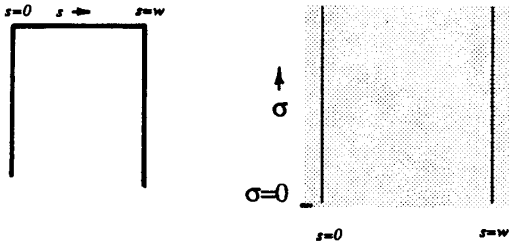

Fig. 8. Right-angle END model and its persistent and stationary scale space map.

space map of the model determined analytically by solving the curvature optimization equation is shown in Fig. 8. □

Property 4: An isolated END model, with $\theta_l = \theta_r = \theta > 0°$ and a corner separation w, has a scale space map symmetric with respect to $w/2$. At $0 \leq \sigma < \sigma_b$, the two absolute maxima move towards each other as σ increases. At $\sigma \geq \sigma_b$, the two absolute maxima merge, forming a single stationary and persistent scale space map.

Let $L(s, \sigma)$ be the left and $R(s, \sigma)$ the right terms of (4.11), respectively. For a particular $\theta_l = \theta_r = \theta$ and at $\sigma = 0$, the two solutions of $L(s, \sigma) = R(s, \sigma)$ are at $s_l = 0$ and $s_r = w$, where w is the corner separation. Note that $s_l(\sigma)$ and $s_r(\sigma)$ are the left and right solutions as a function of σ, respectively. At $0 < \sigma < \sigma_b$, the two solutions $s_l(\sigma)$ and $s_r(\sigma)$ merge toward each other as σ increases, where σ_b is the critical smoothing parameter at which the two corners merge into one because of smoothing. In other words, when $\sigma \geq \sigma_b$, there is only one solution at $s = s_b = w/2$. The merging of $s_l(\sigma)$ and $s_r(\sigma)$ is at $(s, \sigma) = (s_b, \sigma_b)$, which is illustrated in Figs. 9 and 10.

Furthermore, it has been shown that the critical smoothing parameter σ_b depends on θ. The two corners of the END model with large θ merge sooner than those of another END model with small θ. As seen in Fig. 11, one of the solutions $s_l(\sigma)$ moves toward the center of the model as θ increases. □

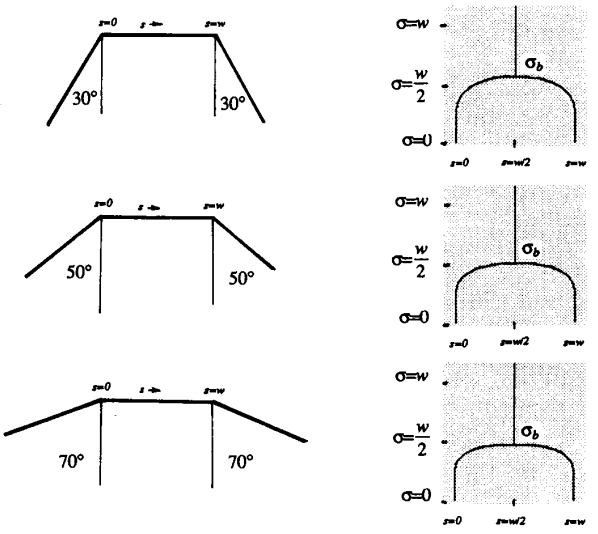

Fig. 9. END model with $\theta_l = \theta_r$. Three examples (30°, 50°, and 70°) are shown.

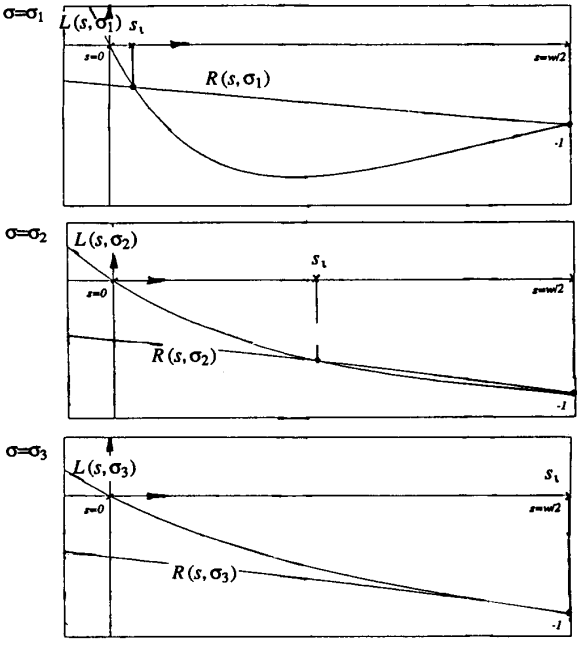

Fig. 10. Merging of corners of the END model with $\theta_l = \theta_r$. $L(s, \sigma)$ and $R(s, \sigma)$ of (4.12) are plotted with the same given w and θ. At $\sigma = \sigma_1$, the top figure shows one of the solutions s_l, which is near $s = 0$; the middle figure shows s_l moving towards $s = w/2$ for a larger $\sigma = \sigma_2$; the bottom figure shows the merging of s_l with $s = w/2$ at $\sigma = \sigma_0$. Note that $\sigma_1 < \sigma_2 < \sigma_0$.

Furthermore, it has been shown that the critical smoothing parameter σ_b depends on θ. The two corners of the END model with large θ merge sooner that those of another END model with small θ. As seen in Fig. 11, one of the solutions $s_l(\sigma)$

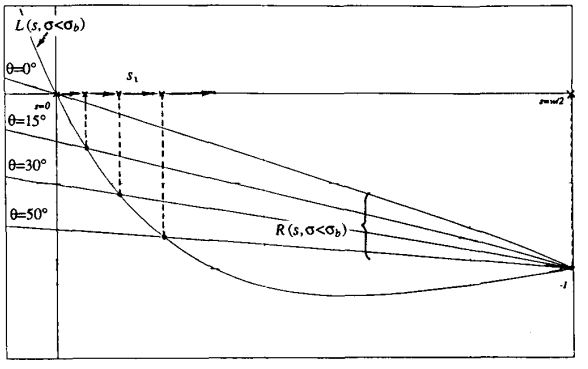

Fig. 11. Merging of corners of the END model with $\theta_l = \theta_r = \theta$. At a given $\sigma < \sigma_b, R(s,\sigma)$ at various values of θ are plotted. The maximum of a large θ is closer to $s = w/2$ than that of a small θ.

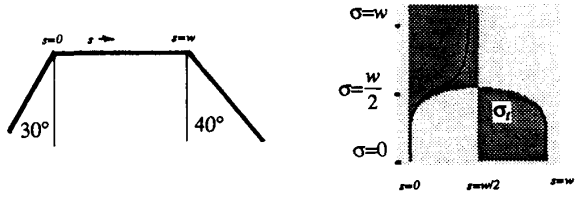

Fig. 12. END model with $\theta_l + \theta_r > 0°$. An example with $\theta_l = 30° < \theta_r = 40°$ is shown. The merging scale space patterns bounded by regions indicated by the shaded areas are shown. The line patterns correspond to the actual scale space map of the model.

moves toward the center of the model as θ increases. □

Property 5: For an isolated END model with $\theta_l < \theta_r$ and $\theta_l + \theta_r > 0°$, the scale space line pattern of the weak corner θ_r terminates at some σ_1 whereas the pattern of the strong corner θ_l persists. Both line patterns move towards the midpoint of the two corners as σ increases.

For an END model that consists of two sides that never intersect, that is, $\theta_l + \theta_r > 0°$ (see Fig. 7), Property 5 states that the sharper corner of the two becomes a single persistent corner, and the weaker one terminates after a finite amount of smoothing. An example is presented in Fig. 12. It is interesting to note that at the point of termination of the weak corner, the maximum of absolute curvature becomes a minimum of absolute curvature. Furthermore, the scale space line patterns of this particular model are bounded by the scale space patterns of 1) a Γ model with a corner at $s = 0$, 2) a Γ model with a corner at $s = w/2$, and 3) an END model with corners at $s = 0$ and $s = w$ both equal to $1/2\,(\theta_l + \theta_r)$. Therefore, the line pattern of the weak corner must terminate at some σ_t, whereas that of the strong corner persists. Moreover, both corners move towards $\sigma = w/2$, where w is the corner separation. The line patterns are bounded within the shaded areas, as shown in Fig. 12. □

Property 6: An isolated END model, with $\theta_l = \theta_r = \theta < 0°$ and a corner separation w has a scale space map symmetric with respect to $w/2$, where the two absolute maxima move away from each other as σ increases.

For the end model with $\theta_l = \theta_r = \theta < 0°$, the two solutions

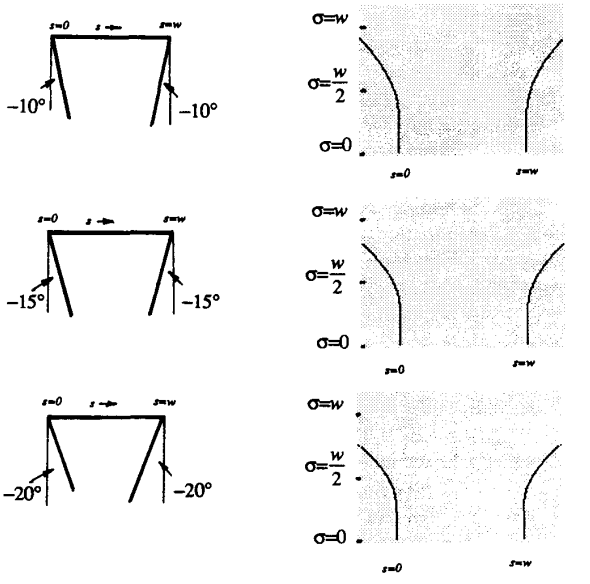

Fig. 13. END model with $\theta_l = \theta_r$. Three examples ($-10°$, $-15°$, and $-20°$) are shown.

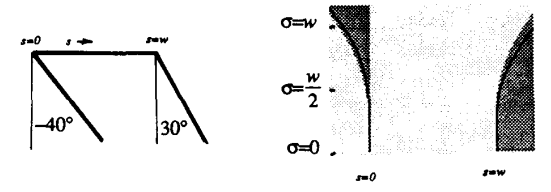

Fig. 14. END model with $\theta_l + \theta_r < 0°$. An example with $\theta_l = -40° < \theta_r = 30°$ is shown. The repelling scale space patterns bounded by the shaded areas are shown. The line patterns correspond to the actual scale space map of the model.

of (4.11) repel each other as σ increases. Fig. 13 contains a number of examples. They show that the solutions originating at $s = 0$ and $s = w$ move away from the center of the model at the same rate as that by which θ decreases.

In an END model whose corner angles are different and $\theta_l + \theta_r < 0°$, the scale space is similar to that described by Property 6; however, the repelling line patterns are no longer symmetric. The scale patterns are bounded by the patterns of 1) the Γ model with a corner at $s = 0$ and 2) the END model with both corners equal to $1/2(\theta_l + \theta_r)$, as shown by the shaded area in Fig. 14. The bounds shows that the weak corner moves away from the center of the model at a faster rate than the strong one as σ increases. □

C. The STAIR Model

The STAIR model, which consists of two corners of opposite concavity separated by a width w, is defined by

$$X(s,0) = \begin{cases} s\,\sin\theta_l & \text{for } s < 0 \\ s & \text{for } 0 \le s < w \\ (s-w)\sin\theta_r + w & \text{for } s \ge w \end{cases} \quad (4.13)$$

$$Y(s,0) = \begin{cases} s\cos\theta_l & \text{for } s < 0 \\ 0 & \text{for } 0 \le s < w. \\ (s-w)\cos\theta_r & \text{for } s \ge w \end{cases} \quad (4.14)$$

Using the Gaussian convolution equations and the above model equations, the curvature optimization of (4.1) becomes the equation shown on the bottom of the page.

The absolute maxima of the above implicit equation at various values of σ form the scale space map. The solution depends on the corner separation w and the corner angles θ_l and θ_r.

Property 7: The scale space map of an isolated STAIR model with corner separation w_i is linearly related to the scale space map of another STAIR model with corner separation ω_j by the ratio of the separations given by w_i/w_j.

This property is similar to Property 2 of the END model. □

Property 8: An isolated STAIR model with corner separation w always produces a persistent scale space map whose two absolute maxima repel each other as σ increases. At $\theta_l = \theta_r = \theta$, the scale space map is symmetrical with respect to $w/2$ independent of θ. At $\theta_l \neq \theta_r$, the weaker corner repels at a faster rate than the strong one as σ increases.

The analysis that leads to the above property is straightforward and is largely omitted here. The repelling of the absolute maxima is illustrated in Fig. 15. At $\theta_l < \theta_r$, the scale space patterns are bounded by the line patterns of 1) the Γ model with a corner at $s = 0$ and 2) the STAIR model with both corners equal to $1/2\,(\theta_l + \theta_r)$. Therefore, the line pattern of the weak corner repels at a faster rate than the strong one as σ increases. In Fig. 15, the shaded areas are used to indicate the bounds. □

D. Planar Closed Curves

From the isolated corner model analysis described in previous sections, it has been observed that each scale space line pattern must either 1) persist, 2) terminate, 3) repel, 4) attract, or 5) merge with a neighboring line. Moreover, new additional lines will not be introduced as σ increases, a fact which agrees with the work by [4]. These properties are verified in this section using planar closed curves.

A closed plane figure at the $\sigma = 0$ level is modeled by a polygon. Each pair of adjacent corners of the polygon is represented by either an END or a STAIR model that possesses the scale space properties as presented in the previous sections. In principle, the scale space of a closed curve is different from that of isolated corner models. In an isolated corner model, each Gaussian smoothing function is assumed to have infinite extent, that is, $-\infty < s < \infty$, and the scale ranges from $\sigma = 0$ to $\sigma = \infty$. In contrast, the coordinate functions $x(s)$ and $y(s)$ of a closed curve are of finite duration; therefore, at each σ, the smoothing function must be of finite extent that will not exceed the length of the curve in order to avoid aliasing.

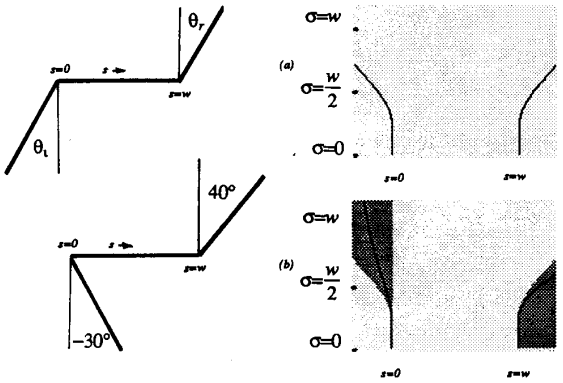

Fig. 15. Repelling maxima of the STAIR model: (a) $\theta_l = \theta_r$ and its symmetric scale space; (b) $\theta_l \neq \theta_r$. An example with $\theta_l = -30° < \theta_r = 40°$ and its corresponding scale space is shown. The line pattern of θ_r repels at a faster rate than that of θ_l. Both line patterns are bounded by the shaded areas.

A number of simple closed curves presented in Fig. 16 was used for the generation of scale space maps. First, the smoothing Gaussian function was cut off (set to zero) beyond three standard deviations to have an extent of six standard deviations. This limits the scale to range from $\sigma = 0$ to $\sigma = S/6$, where S is the total perimeter arc length of the curve. This finite-extent smoothing window well represents the Gaussian function; larger extents were used, and the resulting maps were insensitive to the choice of the extent. Using this modification, the set of closed curves was analyzed to produce the corresponding scale space maps as shown. Although a corner in a closed contour is affected by more than just the nearest neighboring corner, the results in Fig. 16 show that the scale space behavior of the corners in a closed contour is in agreement with that of the isolated corner models in which the effects of faraway corners are neglected.

V. Digital Curve, Digital Curvature, and Digital Scale Space

For digital implementation, it is necessary to define the digital boundary, the curvature measure of the digital curve, and the digital scale space. Let us represent the coordi-

$$\frac{\dot{g}(s,\sigma)}{\dot{g}(s-\omega,\sigma)} = \frac{-\cos\theta_r\left\{1 - 2\int_{-\infty}^{0} g(u-s,\sigma)\,du\right\} - \{\cos\theta_r + \sin\theta_l\cos\theta_r - \cos\theta_l - \sin\theta_r\cos\theta_l\}\int_{-\infty}^{0} g(u-s,\sigma)\,du}{\cos\theta_l\left\{1 - 2\int_{-\infty}^{\omega} g(u-s,\sigma)\,du\right\} - \{\cos\theta_l + \sin\theta_r\cos\theta_l - \cos\theta_r - \sin\theta_r\cos\theta_l\}\left\{1 - \int_{-\infty}^{w} g(u-s,\sigma)\,du\right\}} \quad (4.15)$$

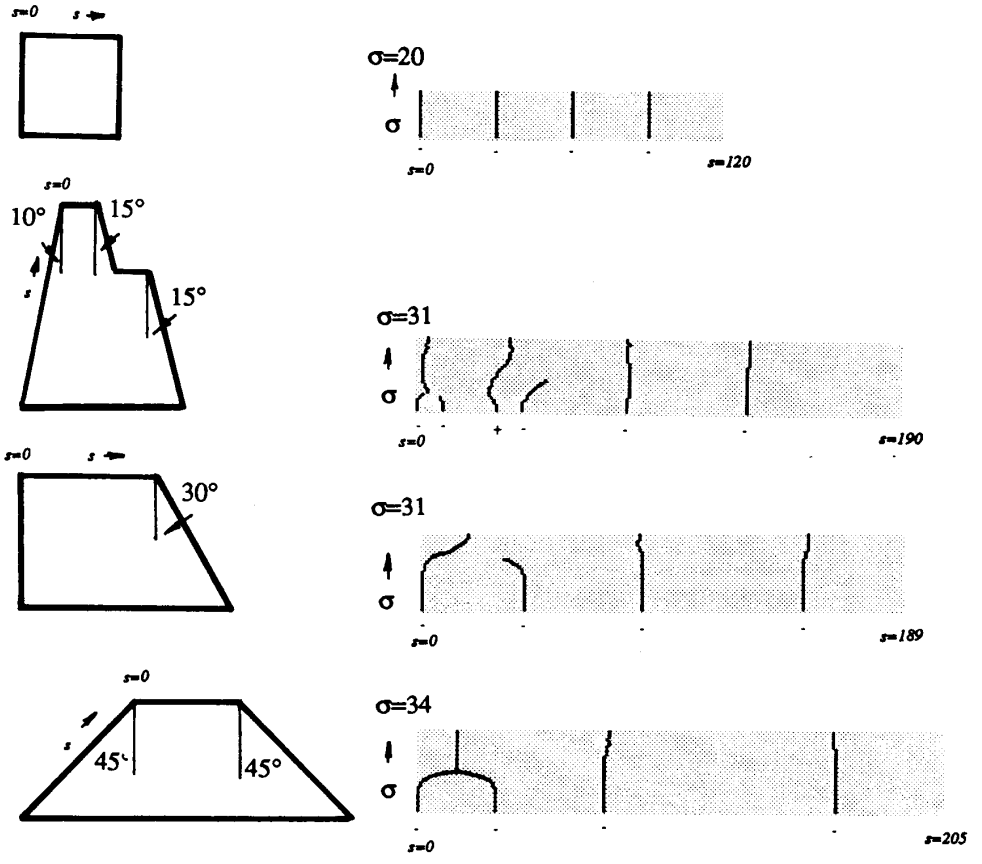

Fig. 16. Closed curves and their corresponding scale space maps.

nate functions $x(s)$ and $y(s)$ of a closed curve digitally by a set of equally spaced Cartesian grid samples $\{x_i, y_i\}$ for $i = 1, 2, \ldots, n$ (modulo n). The curvature measure at point i on the curve can be computed by

$$C_i = \Delta x \Delta^2 y - \Delta y \Delta^2 x \tag{5.1}$$

where Δ denotes the difference operator given by

$$\Delta x_i = \frac{x_{i+1} - x_{i-1}}{\sqrt{(x_{i+1} - x_{i-1})^2 + (y_{i+1} - y_{i-1})^2}} \tag{5.2a}$$

and

$$\Delta y_i = \frac{y_{i+1} - y_{i-1}}{\sqrt{(x_{i+1} - x_{i-1})^2 + (y_{i+1} - y_{i-1})^2}}. \tag{5.2b}$$

The operator Δ^2 is the second-order difference defined by (5.3a) and (5.3b) as shown at the bottom of the page. Note that $(\Delta x)^2 + (\Delta y)^2 = 1$, which is analogous to the condition specified in (3.4).

The digital Gaussian function in [5] with a window size of $K = 3$ is used here to generate smoothing functions at various

$$\Delta^2 x_i = \frac{\frac{x_{i+1} - x_i}{\sqrt{(x_{i+1} - x_i)^2 + (y_{i+1} - y_i)^2}} - \frac{x_i - x_{i-1}}{\sqrt{(x_i - x_{i-1})^2 + (y_i - y_{i-1})^2}}}{\sqrt{\left[1/2(x_{i+1} + x_i) - 1/2(x_i + x_{i-1})\right]^2 + \left[1/2(y_{i+1} + y_i) - 1/2(y_i + y_{i-1})\right]^2}} \tag{5.3a}$$

$$\Delta^2 y_i = \frac{\frac{y_{i+1} - y_i}{\sqrt{(x_{i+1} - x_i)^2 + (y_{i+1} - y_i)^2}} - \frac{y_i - y_{i-1}}{\sqrt{(x_i - x_{i-1})^2 + (y_i - y_{i-1})^2}}}{\sqrt{\left[1/2(x_{i+1} + x_i) - 1/2(x_i + x_{i-1})\right]^2 + \left[1/2(y_{i+1} + y_i) - 1/2(y_i + y_{i-1})\right]^2}}. \tag{5.3b}$$

values of σ and it is given by

$$h[0] = 0.2236 \qquad h[1] = 0.5477 \qquad h[2] = 0.2236 \quad (5.4)$$

where $h[1]$ is the center value and $\sum_k h[k] = 1$. This digital function has been mentioned in [11] and [6] as the best approximation of the Gaussian distribution. For digital smoothing functions with higher values of σ, the above $K = 3$ function is used in a repeating convolution process. For example, a $K = 5$ smoothing function is obtained by convolving (5.4) with itself once, and a $2(j+1)+1$ digital smoothing function is created by repeating the self convolution process j times.

Let us consider that the digital curve given by $\{x_i, y_i\}$ for $i = 1, 2, \ldots, n$, which has a perimeter arc length of n, and consequently, the digital Gaussian smoothing function with the largest σ for the coarsest boundary representation must have a window size no larger than n in order to avoid aliasing.

A multiscale representation of the digital boundary curve from $\sigma = 0$ to $\sigma_{\max}$ is constructed by the digital Gaussian function defined above. The digital curvature of this set of fine-to-coarse curves is then computed by (5.1)–(5.3). To construct the digital scale space, for each point i, a searching procedure is applied to detect the local maximum of absolute curvature within the region of support given by the sequence $\{|C_l|, \ldots, |C_{i-1}|, |C_i|, |C_{i+1}|, \ldots, |C_r|\}$, where C_i is the curvature of the point in question, and C_l and C_r are the leftmost and rightmost points of the local region of support, respectively. The region of support for each point i is the *largest* possible window containing i in which $|C|$ to both the left and right of i is strictly decreasing. A boundary point is not an absolute maximum if such a region of support cannot be determined for that point. Finally, the detected local absolute curvature maxima at every level of σ are plotted in the s-σ space, forming the digital scale space map.

It is reasonable to believe that some of the detected maxima of absolute curvature of the digital scale space do not correspond to the true corner of the boundary. Although such a point is detected numerically as the local absolute maximum, the measurable digital differences in curvature between the point and its neighbors in the region of support are very small, sometimes approaching machine precision, that is, both $|C_i| - |C_l|$ and $|C_i| - |C_r|$ are positive but approaching zero.

For example, a 22.5° quantized line represented digitally by a sequence of one-pixel-high steps or a sequence of STAIR models will generate a number of numerical maxima of absolute curvature, which are not corners of the boundary. Property 8 states that a STAIR model generates a pair of persistent scale space lines that neither terminate nor merge together. It can easily be seen, using this property, that each STAIR model of the quantized straight line generates a pair of persistent lines with very low curvature measures and that they do not correspond to the true corners of the boundary curve.

Another example of numerical absolute maxima is boundary noise on straight lines. A one-pixel boundary noise point on a horizontal straight line will generate a pair of STAIR models, and, in turn, three numerical maxima of absolute curvature that persist through all scales. The difference in curvature between such an absolute maximum and other points in its region of support is very small, especially at large σ. Although these absolute maxima exist theoretically when the boundary is treated as a continuous function, they should not be treated as valid absolute curvature maxima in the implementation of digital scale space.

In order to construct an accurate digital scale space for corner detection, the problem of false corners associated with quantization and boundary noise is addressed. First, all detected absolute curvature maxima for the construction of the digital scale space are examined. Then, 1) true absolute curvature maxima and 2) numerical absolute maxima detected as a result of noise are encoded differently in the digital scale space forming a *coded digital scale space*. To detect a false absolute maximum, say at i, the region of support based on curvature is first determined, as previously described. Then, the perpendicular distance from the absolute maximum at i to the line passing through the two end points at l and r of the region of support is measured. The maximum at i is considered to be a false absolute maximum if the measured distance is smaller than *one* pixel. This threshold is determined based on the fact that a slanted straight line is quantized into a set of either horizontal or vertical line segments separated by *one*-pixel steps. In addition, we assume that boundary noise is no more than one pixel, and if the noise level is known *a priori*, this threshold can be adjusted accordingly. The maxima of absolute curvature are encoded as dashed lines in the coded digital scale space map. An example of the coded map of a digital curve is given in Fig. 17.

VI. Dominant Point (Corner) Detection

A. Digital Scale Space Organization

To detect corners, that is, high curvature dominant points, it is necessary to transform the coded digital scale space map into an organized and well-defined structure for ease of interpretation. In the following, we present a *tree* organization based on the model properties in Section IV and two assumptions described below; this organization is similar to the one in [21].

A *tree* contains a single root and numerous branches and leaves, which simplifies the representation of the scale space line patterns. A *root* is a line representing an absolute curvature maximum that survives the smoothing process and reaches $\sigma_{\max}$. As σ decreases, a root may 1) split up into two or more branches or leaves or both or 2) reach $\sigma = 0$ without branching, thereby forming a *persistent* root. A *branch* is the connecting path between the root and other parts of the tree structure but is connected neither to $\sigma_{\max}$ nor to $\sigma = 0$. A *leaf* is a special branch that is connected to $\sigma = 0$. A branch may further split up into two or more offspring branches or leaves or both as σ decreases.

The above definition of the tree is based on the properties presented in Section IV. The branching of the tree is a direct result of the END model analysis specified in Properties 4 and 5. The persistent root represents most likely the situation described either by Property 1 of the Γ model or by Property 3 of the END model. All other branching patterns of the tree, which depend on corner angles and corner separations, can

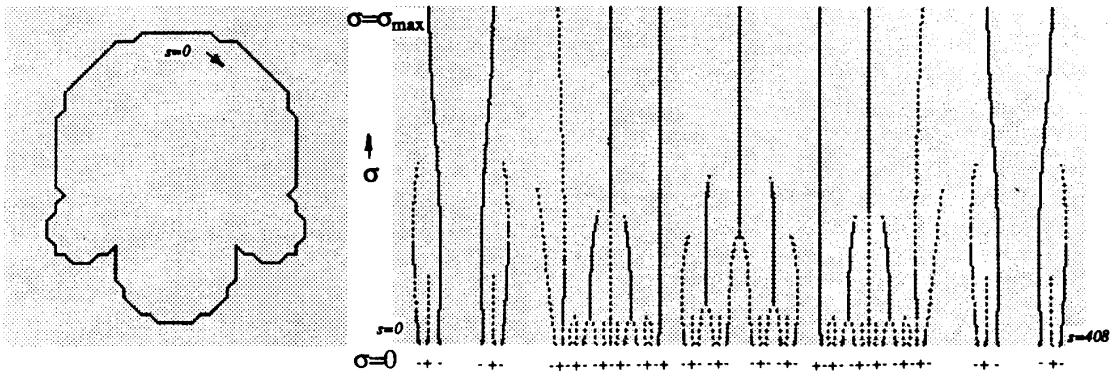

Fig. 17. Digital closed curve and its coded digital scale space map. Solid lines of the scale space map indicate maxima of absolute curvature, and dashed lines indicate numerical maxima due to quantization noise. The + sign indicates downward concavity, and − indicates upward concavity.

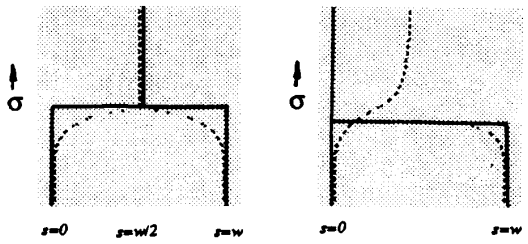

Fig. 18. Tree representations of two END models. The dotted lines represent the digital scale space, and the solid lines represent the tree structures.

be understood by a combination of the properties of the END and STAIR models.

The construction of the tree from the digital scale space map also depends on two assumptions: *identification* and *localization*. These two assumptions are based on effects of smoothing such as the removal of fine features, spatial dislocation, and blurring. The *identification* assumption is obtained from the fact that an absolute curvature maximum observed at different scales forming a continuous line pattern in scale space arises from an underlying evident—the presence of a physical corner observable at various scales *including* $\sigma = 0$. The *localization* assumption states that the true location of the corner giving rise to the scale space pattern is at $(s, \sigma) = (s, 0)$, where the corner is found at the finest scale. Thus, a coarse scale may be used to *identify* corners and a fine scale to *locate* them.

In Fig. 18, two branching patterns are shown that are represented by straight horizontal and vertical lines for ease of interpretation. They are constructed using the model properties in Section IV and the above two assumptions. The left example is a direct result of Property 4 of the END model when two corners become one because of smoothing. The placement of the branches is based on the localization assumption. The right example contains a scale space pattern that has one of the lines terminated at $\sigma = \sigma_t$ as specified by Property 5 of the END model. Its resulting tree contains a root and two leaves linked together at $(s, \sigma) = (s_t, \sigma_t)$. The root is represented by a vertical straight line positioned at the dominating corner observed at $(s, \sigma) = (s_l, 0)$. This notation reflects the localization assumption that the root representing the surviving signal is a product of both corners but with the strong corner dominating the weak one. The construction of a tree is generalized by the following rules.

Rule 1: A root is represented by a vertical straight line located either at the absolute maximum observed at $\sigma = 0$ or at the scale space absolute maxima merging point $\sigma = \sigma_b$. A leaf is a vertical straight line located at the absolute maximum observed at $\sigma = 0$. A branch is a vertical straight line located at the absolute maximum observed at $\sigma = \sigma_b$.

Rule 2: Roots, branches, and leaves are linked together by horizontal straight lines at either the merging scales σ_b or the termination scales σ_t.

Rule 3: A terminating scale space pattern represented by a branch (leaf) links to its nearest neighboring tree structure with the same concavity at σ_t if the branch (leaf) represents an END model observed at σ_t

Rule 4: A terminating scale space pattern represented by a branch (leaf) links to its nearest neighboring tree structure with opposite concavity at σ_t if the branch (leaf) represents a STAIR model observed at σ_t.

The above rules are derived based on the identification and localization assumptions and the fact that the concavity of neighboring scale space patterns differentiates the END model from the STAIR model. Rule 3 governs the tree construction associated with the Property 5 of the END model. Rule 4 is associated with the STAIR model when the STAIR does not survive the smoothing process and is dominated by other neighboring absolute maxima. Note that the information on false absolute maxima due to quantization noise is also encoded in the tree in the same fashion as in the coded digital scale space.

B. Stability Criterion

Scale space line patterns, or their corresponding tree structures, represent both high curvature corners that persist through

a large range of scales and local absolute maxima that appear briefly and vanish after smoothing. For the detection of corners, a *stability* criterion similar to the one in [21] is used to select corners among all the absolute maxima represented by the tree. Stability of a corner is defined as the persistence of its corresponding absolute curvature maximum to withstand smoothing. The stability of each absolute maximum is determined by measuring the length of the corresponding root, branch, or leaf of the tree but excluding the false numerical absolute maxima caused by quantization and noise.

A real physical corner is stable at all scales; therefore, its physical measurement, such as maximum absolute curvature, must be observable at all scales. However, the scale space map of an image is constructed *not* by independent observation of the physical curve at all scales but by Gaussian smoothing of the input boundary function. Therefore, the stability of a corner of an image could only be defined based on *relative* scale persistency. This agrees well with Marr and Hildreth [10] in their edge detection theory in which they state that edges that coincide with each other over several scales are physically significant. Furthermore, Witkin [21] observed empirically that there exists a correspondence between the stability of a feature and its perceptual prominence.

To detect corners from our tree representation, we define a stable corner to be the limp that persists over a *majority* of the scales occupied by a parent and its offsprings. The choice of this 50 *percentile* guarantees the detection of at least one limb among the parent and its offsprings to be a stable corner (but not all of them). This is illustrated in Fig. 18, where two corners at fine scales evolve to become one corner at a coarse scale. In this example, if stability is defined using percentiles other than 50, there will be situations when both the parent and its offspring become stable corners, or no corners are detected at all.

Detection of corners using this stability criterion is described by the following steps:.

Step 1: For each tree, the lengths of its root, branches, and leaves are measured. False numerical absolute maxima are excluded from all measurements.

Step 2: A tree consisting of only a persistent root with a length longer than $1/2\sigma_{\max}$ is considered stable, which corresponds to a corner located at s of the root. Otherwise, there is no corner associated with the tree.

Step 3: For a tree with offspring, the length of the root is compared with the height of its offspring, which is defined as the vertical distance between the branching point σ_b and $\sigma = 0$, excluding false absolute maxima. If the root length is longer than the height of its offspring, the root is declared stable, corresponding to a corner located at s of the root, and the search is completed. Otherwise, the search for stability proceeds to the offspring.

Step 4: If an offspring is a leaf longer than its parent, then it is stable, corresponding to a corner located at s of the leaf.

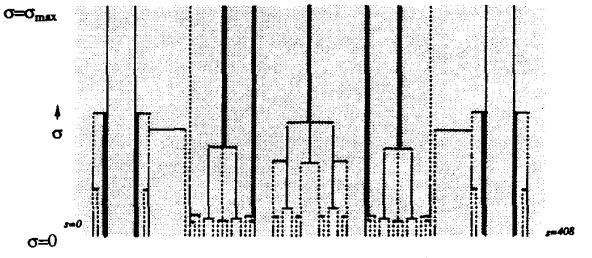

Fig. 19. Stable limbs of the trees are indicated by bold solid lines. The tree represents the object in Fig. 17.

Step 5: If an offspring has its own offspring, the search for stability is applied to this family of the tree, and the process is identical to that applied to the root, as described above, starting from Step 3.

Step 6: This process continues until all branches and leaves are evaluated for possible corners.

The above tree parsing procedure guarantees the determination of no more than one stable limb per s, and each detected corner is more persistent than its descendants and its ancestors. The detected stable limbs of the tree representing the object of Fig. 17 are shown in Fig. 19. The corners are located at s of all the stable limbs.

The above detection procedure is applicable to situations when the freedom for setting a range of scales of interest is desired. This is achieved by replacing $\sigma = 0$ to $\sigma_{\max}$ by a desired range, say σ_a to σ_b. For example, an image of a key could be analyzed at a range of coarse scales by specifying a σ range near $\sigma_{\max}$ or at a fine scales by specifying a range near $\sigma = 0$ to recover the teeth of the key. Experiments are presented in Figs. 26 and 27 in the next section to demonstrate this capability.

VII. Experiments

In this section, we present experimental results of our scale space corner detector. Simple geometric shapes, such as ellipses, squares, and circles were used to test the performance of the detector and its sensitivity to quantization and boundary noise. They were chosen because their dominant points are well defined and can be used as the standard for evaluation. Detected corners other than the known standard sets are considered false detection. In addition, a number of other corner detectors were selected and applied to the same set of test images for comparison purposes.

Fig. 20(a) contains a digital ellipse generated by quantizing its continuous counterpart. Figs. 20(b) and 21(c) contain the corresponding coded digital scale space map and its tree representation, respectively. The detected corners are indicated by • in Fig. 20(a). Two corners were detected corresponding to the end points of the major principal axis. Three other corner detectors (those of Rosenfeld-Johnston [15], Anderson-Bezdek [1], and Teh-Chin [20], were applied to the ellipse in Fig. 20(a). Both the Rosenfeld-Johnston and the Anderson-Bezdek algorithms require input parameters for proper detection; various parameters as suggested in [15] and

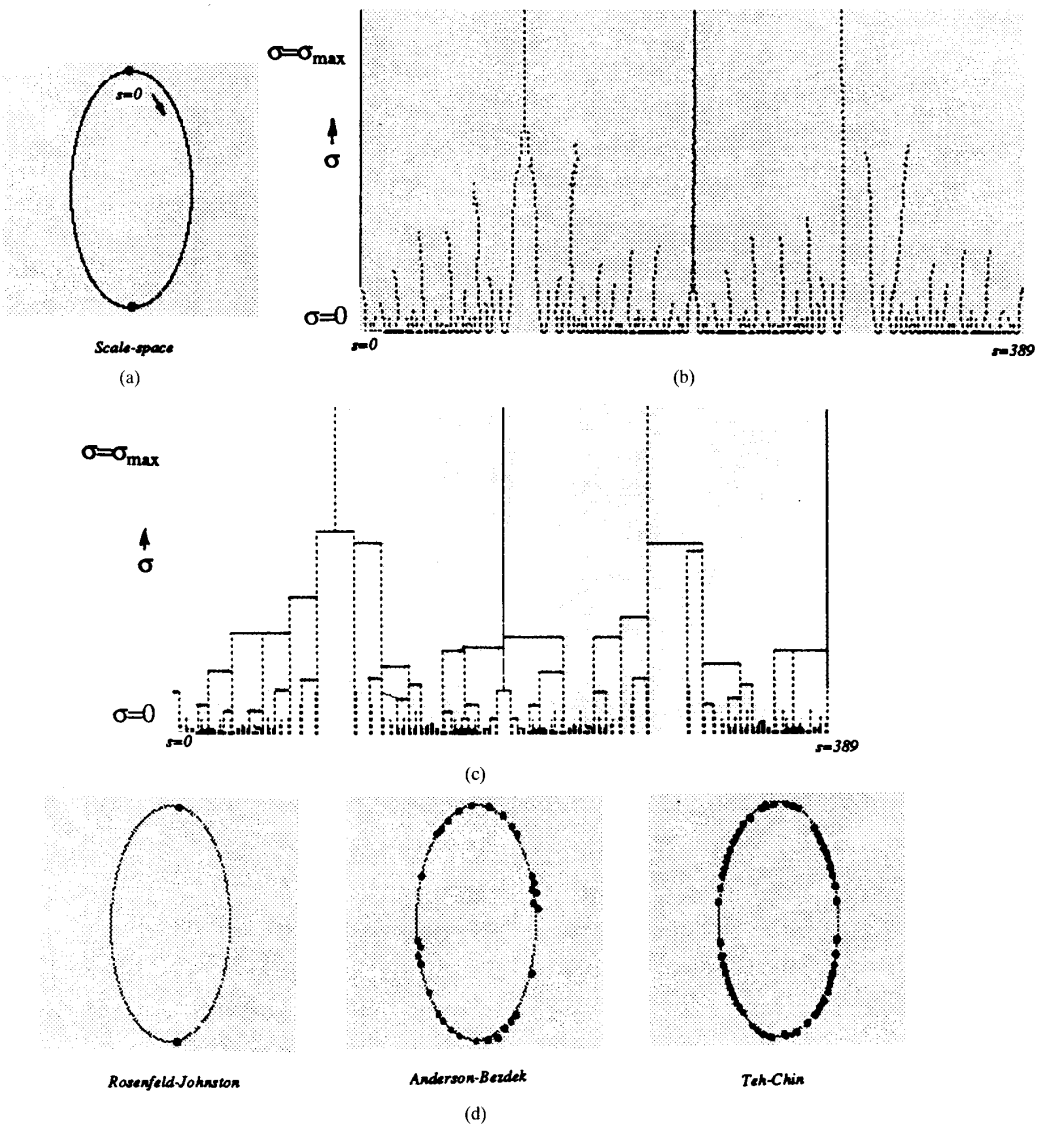

Fig. 20. (a) Digital ellipse with the major and minor axes of 70 and 35 pixels, respectively. The detected corners are indicated by •; (b) corresponding digital coded scale space map; (c) tree representation; (d) corners detected by the Rosenfeld-Johnston, Anderson-Bezdek, and Teh-Chin algorithms.

[1] were tested for the best visual results, as is shown in Fig. 20(d). The statistical approach of the Anderson-Bezdek algorithm does not handle quantization noise well, resulting in a large number of redundant corners. The Teh-Chin algorithm requires no input parameter but results in a large set of redundant dominant points. It is to be noted that these three corner detectors are single-resolution processing algorithms and therefore rely on the information presented at one single scale.

In another experiment, a digital circle was used as the test object; see Fig. 21. Ideally, a circle has identical curvature at every point on the boundary and, therefore, no maximum absolute curvature dominant points. However, our algorithm detected two corners, one on each end of the diameter. A simple post-processing step can be applied to discard these corners, e.g., the application of a threshold based on the curvature at the detected corner, the average curvature of neighboring points, and the boundary noise level. However, such a procedure was omitted for the comparative study to be unbiased. The other algorithms tested resulted in large numbers of dominant points on the digital circle.

The data set used in a study of dominant point detection [20] was used here to further compare our detector with the others. In addition to the three algorithms mentioned above, the corner detectors of Rosenfeld-Weszka [16], Freeman-Davis [17], and Sankar-Sharma [18] were applied to the common test set. A brief description of these algorithms is presented in [20]. The result of the comparison are presented in Figs. 22–25. It is noted that the scale space corner detector compares favorably with the rest.

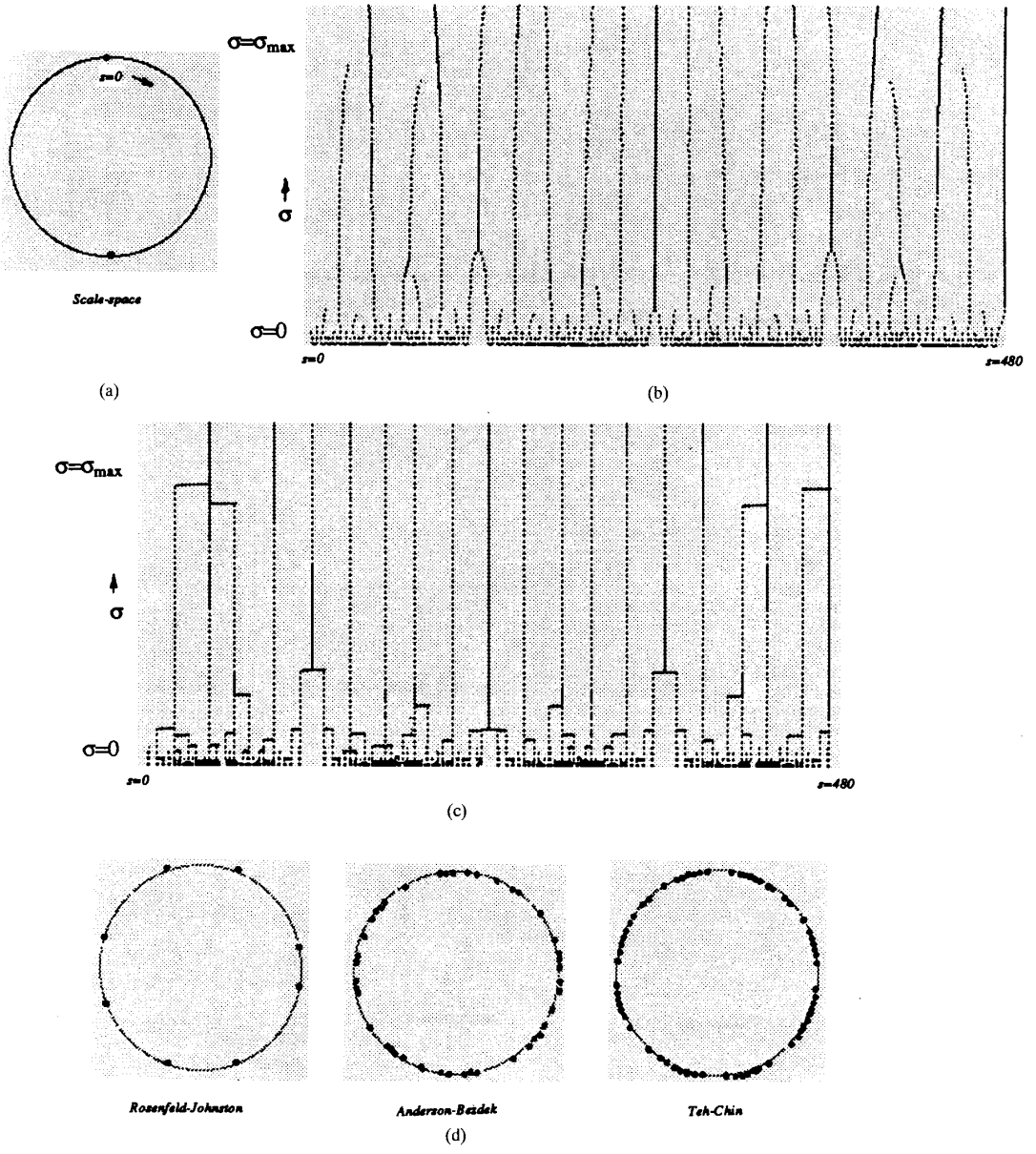

Fig. 21. (a) Digital circle with a radius of 70 pixels. The detected corners are indicated by •; (b) corresponding digital coded scale space map; (c) coded tree representation; (d) corners detected by the Rosenfeld-Johnston, Anderson-Bezdek, and Teh-Chin algorithms.

The proposed corner detector allows the freedom of setting the range of scales of interest. This is demonstrated in two examples in Figs. 26 and 27 in which both test objects consist of multiple-size features. In Fig. 26, the result on the top figure was generated by restricting the parsing of the tree to within a range of coarse scales, indicated by the dark shaded region. As expected, the detected corners describe the general shape of the key without much detail. The result on the bottom figure was generated by selecting a range of fine scales indicated by the light shaded region; the detected corners show all the fine features of the key. In Fig. 27, three ranges of scales were used. The coarse range resulted in the detection of the four corners; the midrange detected additional corners of dominant features; the fine range of scales detected most of the corners.

In order to investigate the sensitivity of the scale space corner detector to boundary noise, a digital square object, roughly 80 × 80 pixels in size, which consists of eight known corners (two concaved upward and six concaved downward) was constructed. Random white noise was added to the object by rounding off white Gaussian noise to the nearest integer and adding it to the digital boundary. Various levels of additive noise with σ_N ranging from 0.5 to 2.5 were used to generate different test cases. In one case of severe noise, a noisy boundary point is at a location 27 pixels from the true object

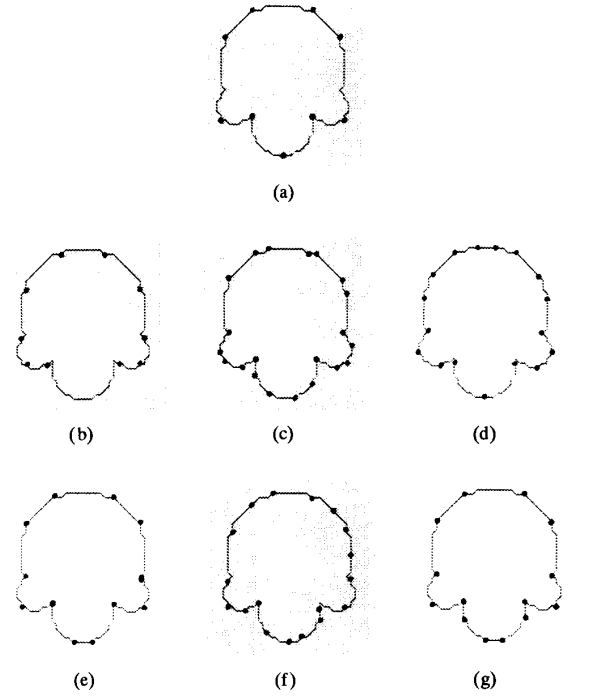

Fig. 22. Digital object consists of one large semi-circle and three small semi-circles. Corners are indicated by •: (a) Scale space corner detector; (b) Sankar-Sharma; (c) Teh-Chin; (d) Freeman-Davis; (e) Rosenfeld-Johnson; (f) Anderson-Bezdek; (g) Rosenfeld-Weazka.

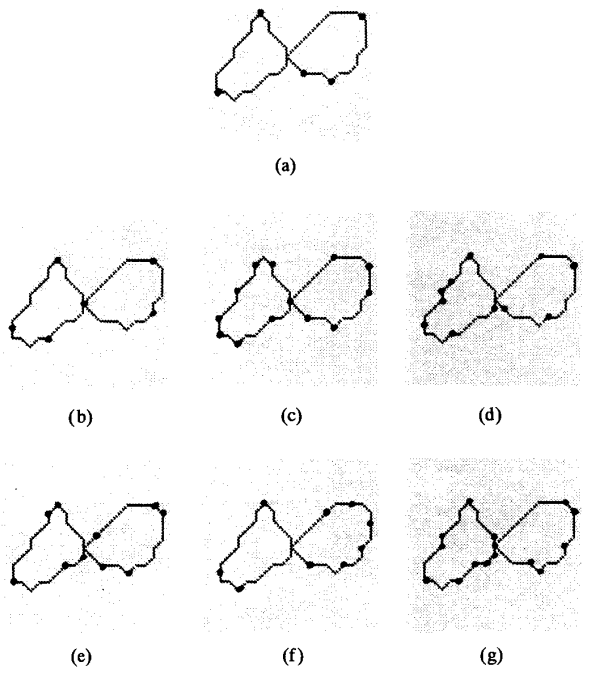

Fig. 24. Digital figure-8 object: Corners are indicated by •: (a) Scale space corner detector; (b) Sankar-Sharma; (c) Teh-Chin; (d) Freeman-Davis; (e) Rosenfeld-Johnson; (f) Anderson-Bezdek; (g) Rosenfeld-Weazka.

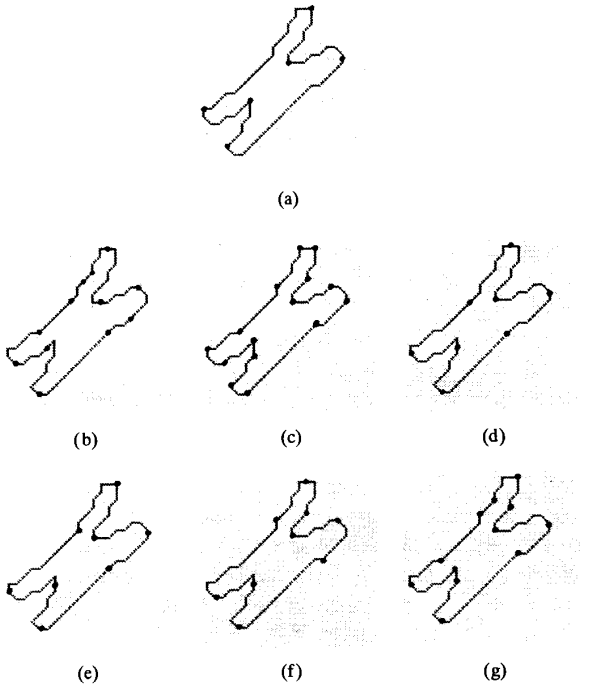

Fig. 23. Digital chromosome: Corners are indicated by •: (a) Scale space corner detector; (b) Sankar-Sharma; (c) Teh-Chin; (d) Freeman-Davis; (e) Rosenfeld-Johnson; (f) Anderson-Bezdek; (g) Rosenfeld-Weazka.

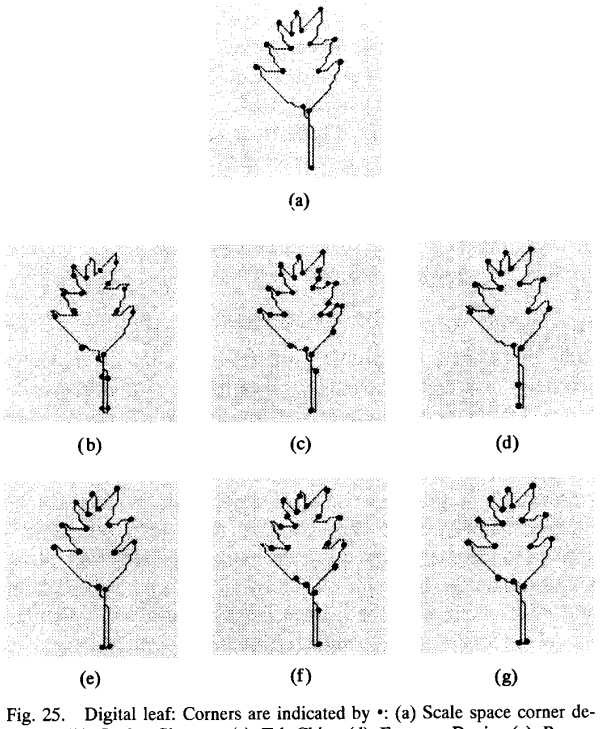

Fig. 25. Digital leaf: Corners are indicated by •: (a) Scale space corner detector; (b) Sankar-Sharma; (c) Teh-Chin; (d) Freeman-Davis; (e) Rosenfeld-Johnson; (f) Anderson-Bezdek; (g) Rosenfeld-Weazka.

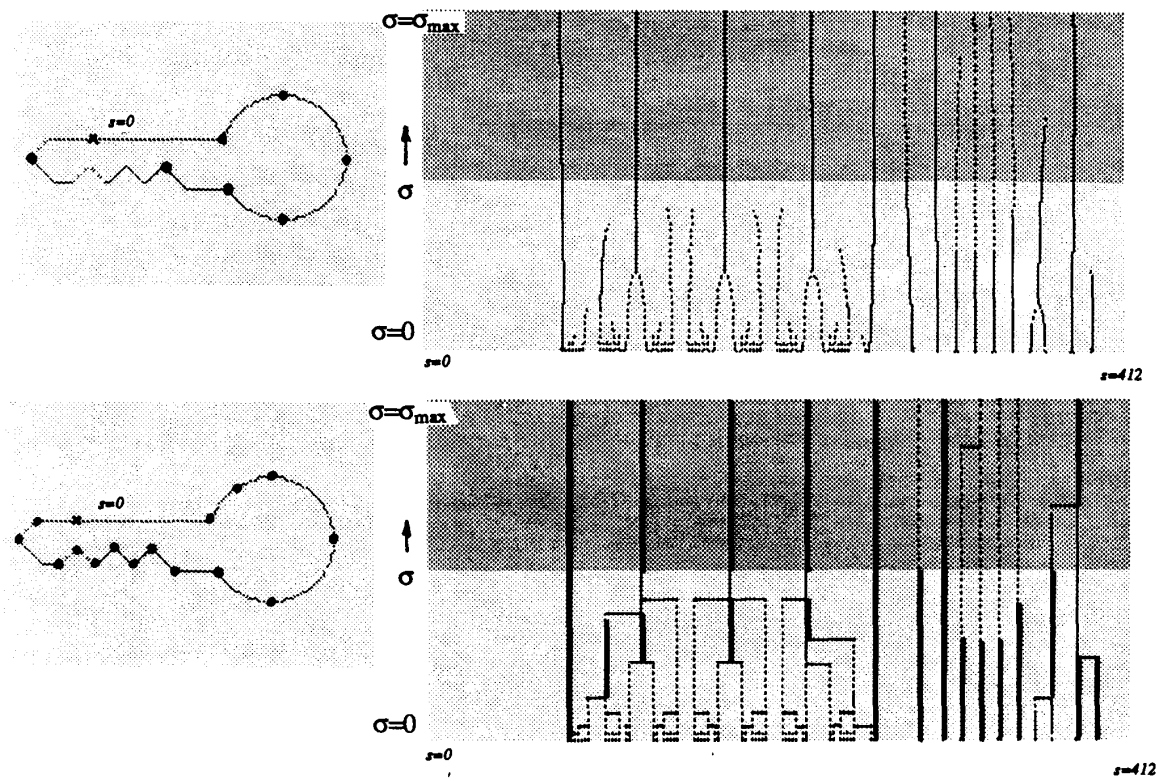

Fig. 26. Restricting the range of scales of interest: Boundary contour of a key, the corresponding scale space, and its tree representation. The dark shaded region corresponds to the range of coarse scales, and the light shaded region corresponds to the range of fine scales. Top figure: Corners detected from the coarse range of scales. Bottom figure: Corners detected from the fine range of scales.

boundary. The various test cases, their corresponding coded digital scale space maps, and the detected corners are shown in Fig. 28. The result shows that the detected corners are quite consistent, even at high noise levels.

In another experiment, a gray-level image of a wrench was used. Edge detection was first applied to generate a binary edge image. Then, the outer boundary of the wrench was extracted, and contour following was applied to produce the closed curve that was inputted to the scale-based corner detector. Detected corners are shown in Fig. 29.

VIII. Conclusions

In this paper, the problem of detecting dominant points (corners) of a digital boundary curve based on multiple-scale representation and searching was investigated. A scale space map of absolute curvature maxima, which contains locations of maxima of absolute curvature of the boundary, was constructed. A number of isolated simple and double corner models, namely, the Γ, END, and STAIR, were defined and applied to the analysis of the scale space map. They were used to determine the behavior of a corner due to both smoothing and interactions with the nearest neighboring corner. Various model properties were specified, from which conclusions have been reached that each line pattern of the scale space either persists, terminates, or merges with a neighboring pattern. Moreover, new additional line patterns will not be introduced by smoothing.

Digital implementation of the scale space was proposed in which the model properties are preserved. In order to alleviate problems of quantization noise associated with digital boundary lines, the digital scale space was encoded to indicate false absolute maxima resulting from quantization. Subsequently, the coded scale space was transformed into a tree representation for the detection of corners. A stability criterion was adopted to search for stable absolute maxima through all scales, or at a specific range of scale of interest, where the locations of these stable absolute maxima are considered to be corners.

Experiments were conducted to show the effectiveness of this scale space corner detector. First, a set of simple geometric objects with known corner locations was used as bench marks in a testing procedure. Next, a set of objects, commonly used in other corner detection studies, was used in another experiment to compare the scale space corner detector with a number of others. The experiments have shown that our detector compares favorably with other existing corner detection algorithms. Then, the detector was applied to noisy objects and was shown to be quite reliable, even in the presence of severe boundary noise. Finally, the detector was tested using gray-level image; the result was reliable.

However, it has been observed from some of the experimental results that the proposed scale space procedure also detects false corners (e.g., corners on a circle). This is due to

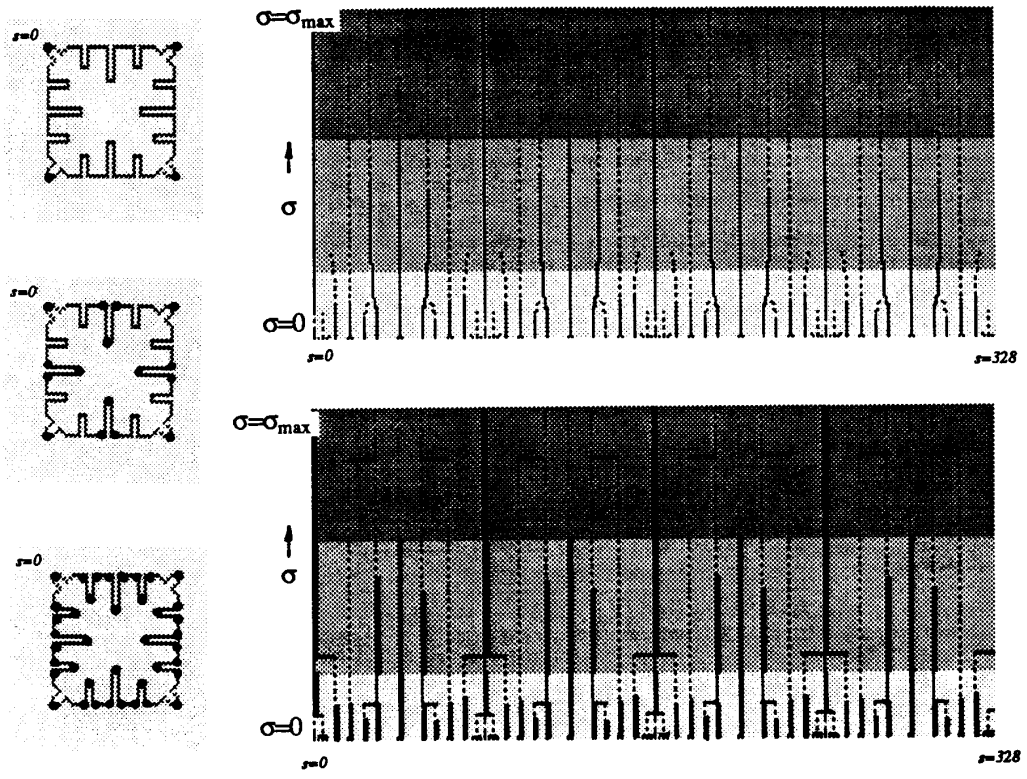

Fig. 27. Restricting the range of scales of interest: Boundary contour of a snowflake, the corresponding scale space, and its tree representation. The darkest shaded region corresponds to the range of coarse scales, and the lightest shaded region corresponds to the range of fine scales. Top figure: Corners detected from the coarse range of scales. Bottom figure: Corners detected from the fine range of scales.

quantization noise and the fact that only locations of curvature maxima are used in the map to detect true corners and to eliminate noise. This suggests the use of other features for the construction of scale space and the detection of corners. One potential feature for the scale space is the curvature magnitude, which could be interpretated as the strength of a curvature maximum. This feature could be used to classify corner types and to eliminate false detection. This feature and other new features for scale space processing are under investigation.

REFERENCES

[1] I. M. Anderson and J. C. Bezdek, "Curvature and tangential deflection of discrete arcs: A theory based on the commutator of scatter matrix pairs and its application to vertex detection in planar shape," *IEEE Trans. Patt. Anal. Machine Intell.*, vol. PAMI-6, no. 1, pp. 27–40, Jan. 1984.

[2] H. Asada and M. Brady, "The curvature primal sketch," *IEEE Trans. Patt. Anal. Machine Intell.*, vol. PAMI-8, no. 1, pp. 2–14, Jan. 1986.

[3] F. Attneave, "Some informational aspects of visual perception," *Psychol. Rev.*, vol. 61, no. 3, pp. 183–193, 1954.

[4] J. Babaud, A. P. Witkin, M. Baudin, and R. O. Duda, "Uniqueness of the Gaussian kernel for scale-space filter," *IEEE Trans. Patt. Anal. Machine Intell.*, vol. PAMI-8, no. 1, pp. 26–33, 1986.

[5] P. J. Burt, "Fast filter transform for image processing," *Comput. Vision Graphics Image Processing*, vol. 16, pp. 20–51, 1981.

[6] P. J. Burt and E. H. Adelson, "The Laplacian pyramid as a compact image code," *IEEE Trans. Commun.*, vol. COM-31, no. 4, Apr. 1983.

[7] J. J. Clark, "Singularity theory and phontom edges in scale space," *IEEE Trans. Patt. Anal. Machine Intell.*, vol. PAMI-10, no. 5, pp. 720–727, 1988.

[8] H. Freeman and L. S. Davis, "A corner-finding algorithm for chain-coded curves," *IEEE Trans. Comput.*, vol. C-26, pp. 297–303, Mar. 1977.

[9] D. Langride, "On the computation of shape," in *Frontiers of Pattern Recognition* (S. Watanabe, Ed.) New York: Academic, 1972, pp. 347–365.

[10] D. Marr and E. C. Hildreth, "Theory of edge detection," *Proc. Roy. Soc. London B*, vol. 270, pp. 187–217, 1980.

[11] P. Meer, E. S. Baugher, and A. Rosenfeld, "Frequency domain analysis and synthesis of image pyramid generating kernels," *IEEE Trans. Patt. Anal. Machine Intell.*, vol. PAMI-9, no. 4, pp. 512–522, 1987.

[12] ——, "Extraction of trend lines and extrema from multiscale curves," *Pattern Recogn.* vol. 21, no. 3, pp. 217–226, 1988.

[13] F. Mokhtarian and A. Mackworth, "Scale-based description and recognition of planar curves and two-dimensional shapes," *IEEE Trans. Patt. Anal. Machine Intell.*, vol. PAMI-8, no. 1, pp. 34–43, Jan. 1986.

[14] M. A. Piech, "Comment on fingerprints of two-dimensional edge models," *Comput. Vision Graphics Image Processing*, vol. 42, pp. 381–386, 1988.

[15] A. Rosenfeld and E. Johnston, "Angle detection on digital curves," *IEEE Trans. Comput.*, vol. C-22, pp. 875–878, Sept. 1973.

[16] A. Rosenfeld and J. S. Weazka, "An improved method of angle detection on digital curves," *IEEE Trans. Comput.* vol. C-24, pp. 940–941, Sept. 1975.

[17] P. Saint-Marc and G. Medioni, "Adaptive smoothing for feature extraction," in *Proc. Image Understanding*, Apr. 1988, pp. 1100–1113, vol. II.

[18] P. V. Sankar and C. V. Sharma, "A parallel procedure for the detection of dominant points on a digital curves," *Comput. Vision Graphics Image Processing*, vol. 7, pp. 403–412, 1978.

[19] M. Shah, A. Sood, and R. Jain, "Pulse and staircase edge models," *Comput. Vision Graphics Image Processing*, vol. 34, pp. 321–343, 1986.

[20] C. Teh and R. T. Chin, "On the detection of dominant points on digital curves," *IEEE Trans. Patt. Anal. Machine Intell.*, vol. PAMI-11, no. 8, pp. 859–872, Aug. 1989.

[21] A. P. Witkin, "Scale-space filtering," *Proc. 8th Int. Joint Conf. Artificial Intell.* (Kalsruhe, West Germany), 1983, pp. 1019–1021.

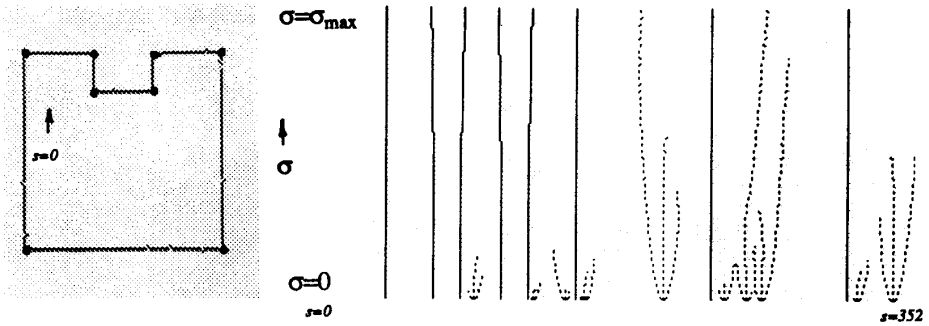

(a)

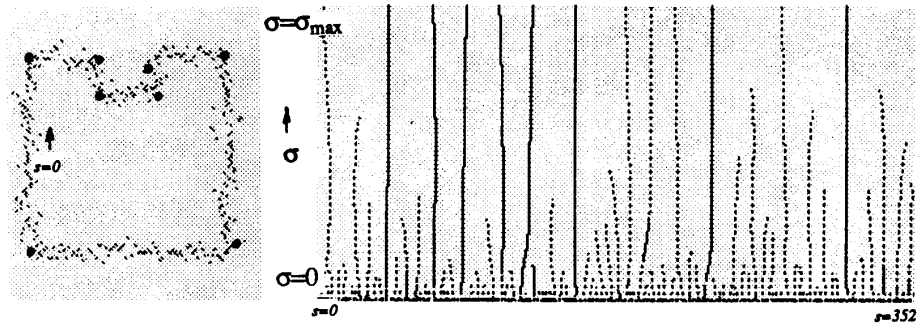

(b)

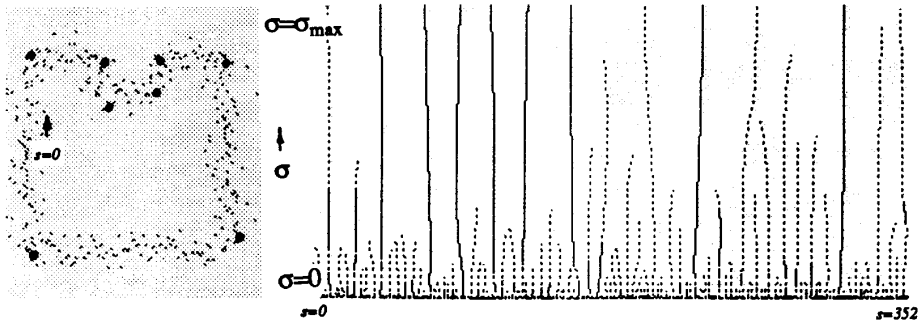

(c)

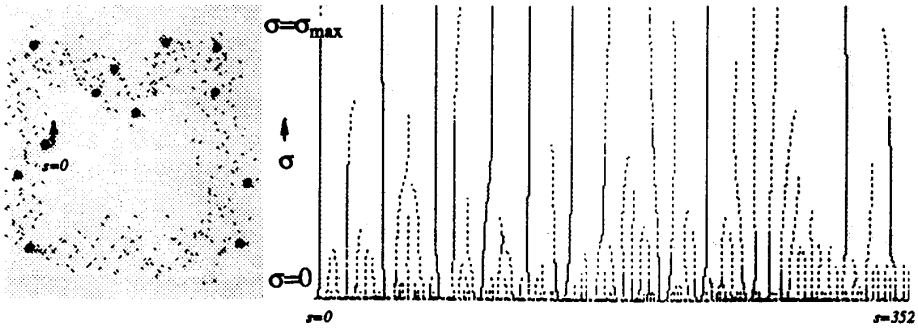

(d)

Fig. 28. Noise sensitivity. The left column shows four square objects each at a different level of added random Gaussian noise of, from top to bottom, $\sigma_N =$ (a) 0.5, (b) 1.5, (c) 2.0, and (d) 2.5. Detected corners are indicated by •. The right column shows their corresponding coded digital scale space maps.

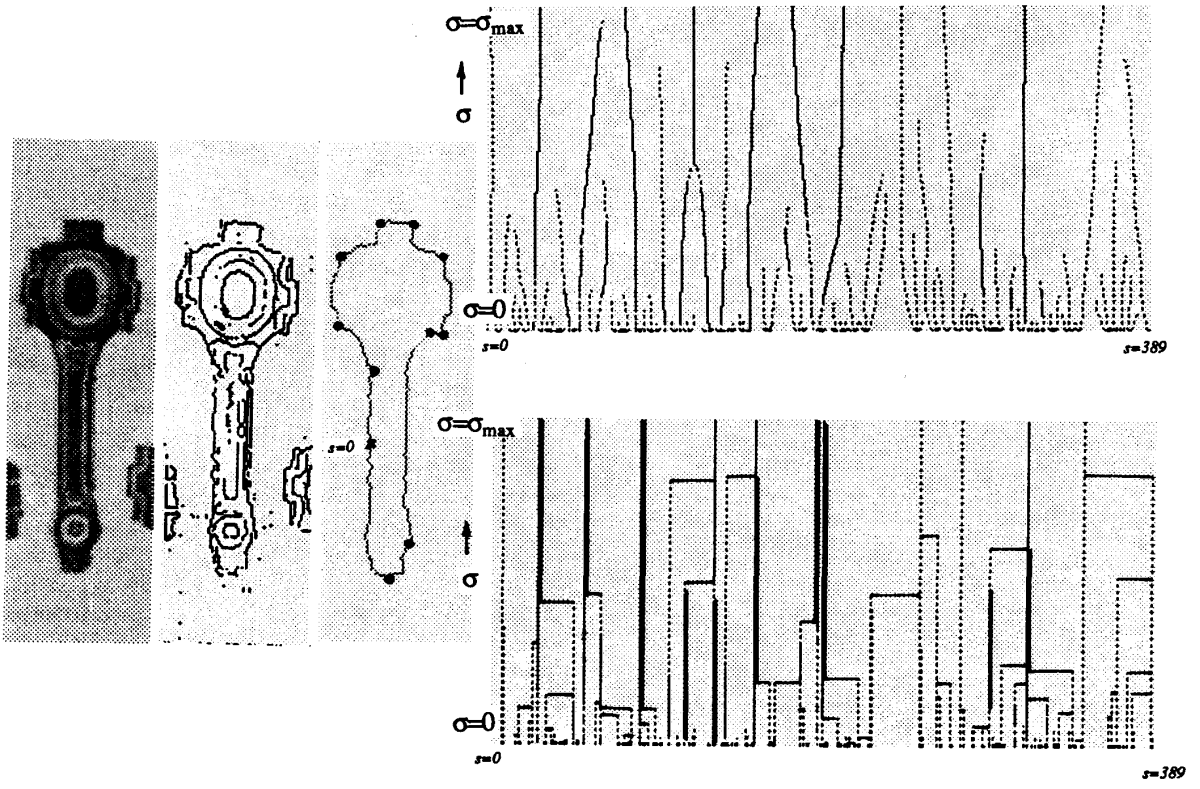

Fig. 29. Corners of a wrench. Left: Gray-level image. Middle: Edge map. Right: Closed curve of the outer boundary and the detected corners indicated by •. The scale space map, the tree, and the stable limbs are also shown.

[22] A. L. Yuille and T. A. Poggio, "Scaling theorems for zero-crossings," *IEEE Trans. Patt. Anal. Machine Intell.*, vol. PAMI-8, no. 1, pp. 15–25, Jan. 1986.

Anothai Rattarangsi received the Ph.D. degree in 1991 in electrical engineering from the University of Wisconsin-Madison, where he also received the B.S. (Honors) and M.S. degrees.

He is currently the director of the Research Center in the Electrical and Electronic Department, the Royal Thai Navy, Thailand. He is also a visiting lecturer at several universities in Bangkok. His primary areas of interest include multiscale approaches, motion, data compression, and recognition.

Roland T. Chin received the B.S. degree with honors in 1975 and the Ph.D. degree in 1979 in electrical engineering from the University of Missouri, Columbia.

From 1979 to 1981, he was involved in remote sensing research for NASA Goddard Space Flight Center, Greenbelt, MD. Since 1981, he has been on the faculty of the Department of Electrical and Computer Engineering at the University of Wisconsin, Madison, where he is currently a Professor. His current research interests include image restoration, texture analysis, shape descriptions, pattern recognition, visual inspection, object recognition, and related applications.

Dr. Chin is a member of Eta Kappa Nu and Tau Beta Pi, and he was the recipient of the Presidential Young Investigator Award in 1984. He is on the editorial board of *Asia-Pacific Engineering Journal* and is an Associate Editor of IEEE TRANSACTIONS ON IMAGE PROCESSING.